# Literature review

## 1.1 Introduction

Plasma spraying is the part of thermal spraying, which according to the definition given by American Society of Materials (ASM) is a group of processes in which finely divided metallic and non-metallic surfacing materials are deposited in a molten or semi-molten condition on a substrate to form a spray deposit [4]. The thermal spraying techniques can be classified according to the energy source and the conditions of the process, what is presented in Figure 1.1.

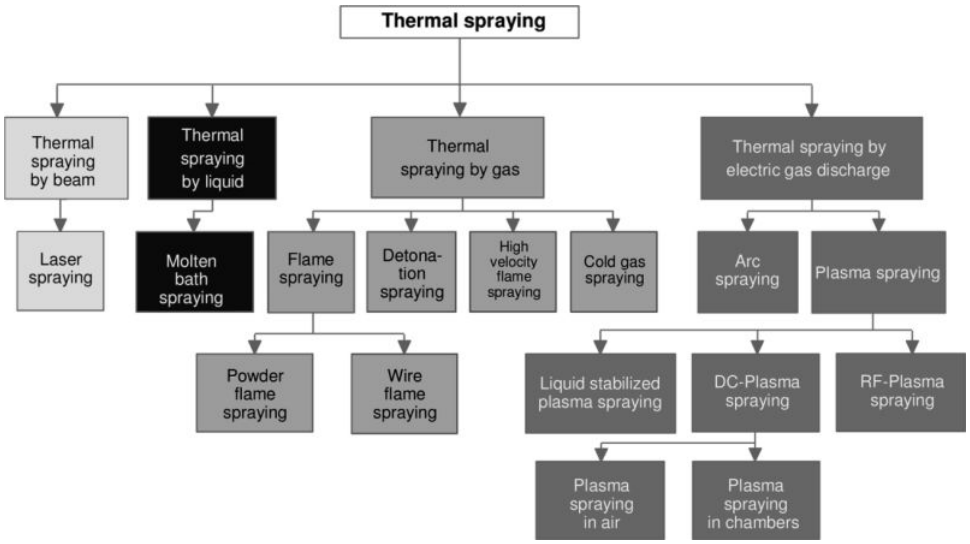


**Figure 1.1:** Overview of the different thermal-spray processes. [4]

This work focuses on the plasma spraying process with the material injected into a direct current (dc) plasma jet at atmospheric pressure (plasma spraying in air in Figure 1.1). Due to feedstock material injected into the plasma jet the plasma spraying technique can be categorized into: atmospheric plasma spraying (APS), solution precursor plasma spraying (SPPS) and suspension plasma spraying (SPS) [5–7]. In the APS process, solid powder particles are injected into the plasma jet. The minimum thickness of the coatings is limited to about 10 $\mu$m [7]. They are mostly used to provide protection against high temperatures, corrosion, erosion and wear. The increasing interest in nanomaterials, which according to the definition given by US National Nanotechnology Initiative are the material structures with at least one dimension smaller than 100 nm, results in the development of new plasma spraying processes. The one of this method, described by Karthikeyan *et al.* [8], is the solution precursor plasma spraying, in which instead of the conventional powder feedstock, an aqueous solution precursor is injected into the plasma jet. This process allows obtaining the nano- and sub-micrometric microstructure of coatings. An alternative method is a relatively new suspension plasma spraying, which has been invented by the University of Sherbrooke in the mid-1990s [9]. The suspension

composed of submicron or nano-sized powder particles suspended in a liquid is used as the feedstock. The SPS process permits to produce finely structured nano-sized coatings, what allows expanding the application area of the plasma spraying method. They may be used as:

- Solid oxide fuel cell (SOFC)
  It is an electrochemical conversion device that produces electricity directly from oxidizing a fuel. It consists of four layers: anode, electrolyte, cathode and interconnect. The three first coatings are ceramic, not electrically and ionically active below about 600°C. Therefore, many efforts have been devoted to produce the coatings for these SOFC components by suspension plasma spraying method. The anode consists of the porous nickel-YSZ (yttria-stabilized zirconia) cermet coating. The electrolyte requires a dense and thin ($< 15$ $\mu$m) YSZ coating. The porous perovskite, e.g. lanthanum ferro-cobaltite doped with strontium (LSCF) or lanthanum manganite doped with strontium (LSM) coating should be produced for the cathode.

- Thermal barrier coating (TBC)
  Thermal barrier coatings (TBCs) are advanced material systems applied to metallic surfaces, e.g. gas turbine or aero-engine parts, to help protect these components from the heat and thermal degradation. The TBC materials should be characterized by: high melting point, low thermal conductivity, thermal expansion match with the metallic substrate, good adherence to the metallic substrate and a low sintering rate of the porous microstructure. Therefore, the number of materials that can be used as TBCs is very limited. The ceramic coatings such as $Al_2O_3$, $TiO_2$, mullite, $ZrO_2$, YSZ, $CeO_2$, $La_2Zr_2O_7$ are applied as TBC materials, among which yttria-stabilized zirconia (YSZ) is the most widely studied [10–12].

- Photo-catalytic coatings
  In recent years the photo-catalysis process has been used in a broad range of applications, including especially environmental and energy-related fields, illustrated in the example of $TiO_2$ photo-catalysis in Figure 1.2.

  Several semiconductors ($TiO_2$, ZnO, $Fe_2O_3$, CdS, ZnS) can act as photocatalysts but $TiO_2$ has been most commonly studied due to its photocatalytic and hydrophilic properties and moreover, high reactivity, reduced toxicity, chemical stability and lower cost. The photo-catalytic properties of $TiO_2$ coating depend on its phase composition. The anatase $TiO_2$ presents a higher photocatalytic activity than its rutile phase. 65 vol.% of anatase is necessary to achieve an acceptable photo-catalytic performance.

However, in more complex applications the researchers face still many problems, such as obtaining the appropriate crystallographic structure of materials.

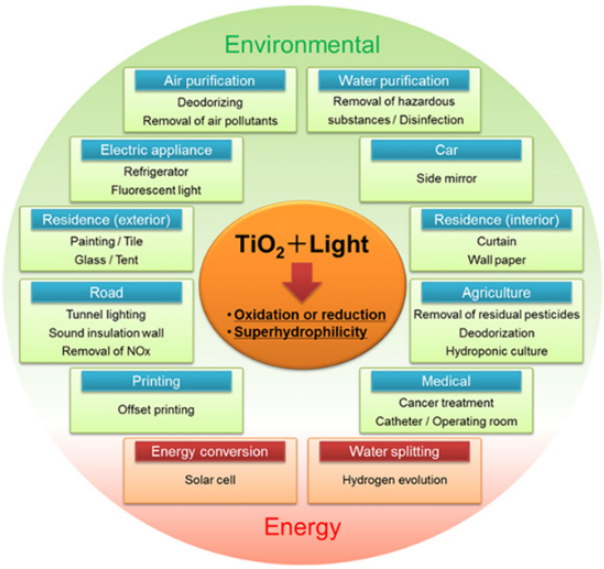


**Figure 1.2:** Applications of $TiO_2$ photo-catalysis [13].

As Henne has presented on the example of solid oxide fuel cells (SOFC), these more complex devices can be produced by other thermal spray methods, such as vacuum plasma spraying (VPS) [14]. However, the goal of technological development is the reduction of costs what can be achieved by suspension plasma spraying using dc torches at atmospheric pressure. Therefore, the following thesis is focused on the studies and the improvement of direct current plasma torch associated with the suspension injection.
In suspension plasma spraying method the material in the form of suspension is introduced into the plasma jet produced by a direct current (dc) plasma torch. This process can be divided into three important phases, indicated in Figure 1.3:

I Plasma production

II Suspension injection and penetration into the plasma jet

III Material deposition

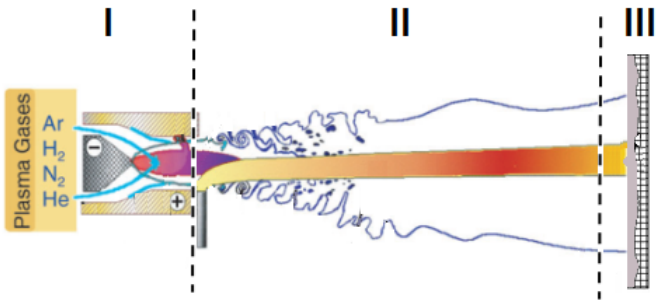


**Figure 1.3:** Schematic view of a plasma spraying method [15].

Therefore, the following paragraph has been divided into three parts.

## 1.2 Fundamentals of plasma spraying process

The plasma, often referred to a fourth state of matter, is a gas electrically conducting due to the presence of charged particles [16–18]. It can be defined as a collection of species: electrons, ions and neutral particles moving in random directions, schematically presented in Figure 1.4. The mass of the ions and neutrals, $m_h$, is much higher than the electron

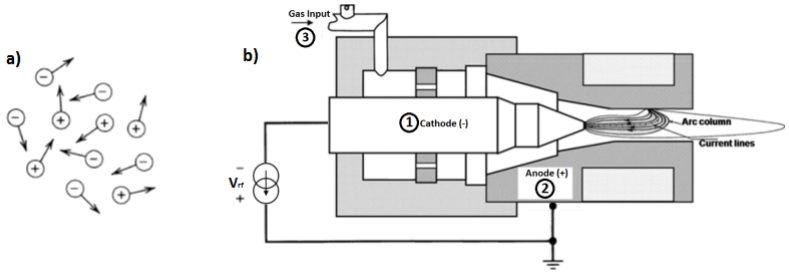


**Figure 1.4:** Schematic view of a) plasma; b) plasma formation by a direct current plasma torch.

mass, $m_e$, therefore, these species have been defined as heavy particles. The plasma is the result of the transformation of gas atoms to charged particles in consequence of the increasing temperature, what can be achieved by different methods, e.g. microwaves, RF discharges, laser. The following thesis is focused on the plasma spraying method. In this technique the plasma is produced by the electric discharge using the direct current (dc) plasma torch, what is presented in the following section.

### 1.2.1 Direct current plasma torch

As mentioned above, in the plasma spraying process the plasma jet is formed in the torch. According to the current terminology, defined by Zukov *et al.*, the term plasma torch indicates the apparatus designed for the production of low temperature plasma by heating the gas using the electric arc [19]. The first industrial dc plasma torches appeared in the 1960s [15]. Since that time, a large number of torch designs has been developed. The differences between the torches consist in various types of the cathode tips, the gas injection, the nozzle shapes and diameters. The basic concept of the plasma torch, shown in Figure 1.5, comprises a cathode, a plasma forming gas injector and an anode nozzle. The following section focuses on the detailed description of a direct current non-transferred plasma torch.

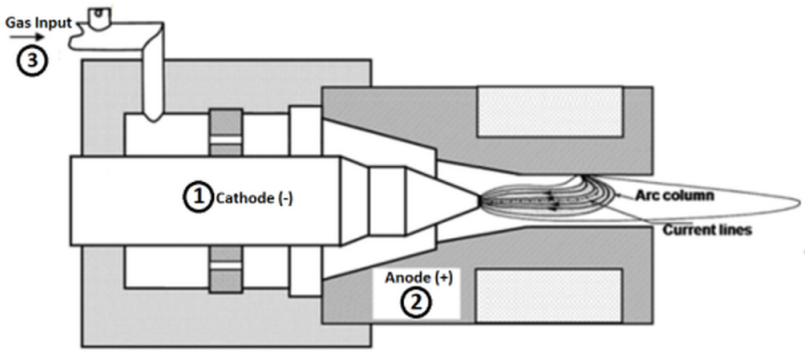


**Figure 1.5:** Schematic view of a direct current plasma torch.

- **Cathode**

It emits the electrons for maintaining the arc discharge. The parameters of the cathode differ according to the electrons emission mechanisms. In the case of the hot cathode (a, b in Figure 1.6) is the thermionic emission defined by Richardson-Dushman law:

$$J = A_G T^2 e^{\frac{-W}{kT}} \tag{1.1}$$

where:

| | |
|---|---|
| $J$ | is the emission current density [A.m$^{-2}$], |
| $T$ | the temperature of the metal, |
| $W$ | the work function of the metal, |
| $k$ | the Boltzmann constant, |
| $A_G$ | the constant defined by: $A_G = \frac{4\pi m k^2 e}{h^3} = 1.20173 \times 10^6$ [A.m$^{-2}$.K$^{-2}$]. |

This type of the cathode is commonly made of tungsten doped with $1-2$ wt% of $ThO_2$; 2 wt% of $La_2O_3$, $Y_2O_3$, $CeO_2$ [20, 21]. The role of the dopant is to lower the thermionic work function of tungsten and therefore, the operating temperature, to which generally the erosion of the cathode is related. Sadek *et al.* have investigated the erosion rates of different cathode materials in 150 A. The $La_2O_3$ doped tungsten electrode is characterized by the lowest operating temperature (2750 K comparing to 3600 K of $ThO_2$) and the lowest erosion rate [22].

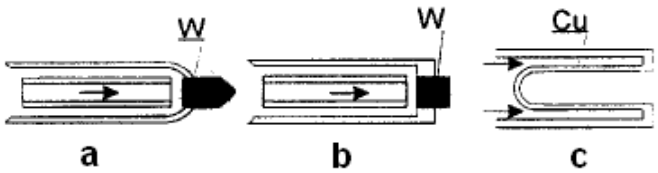


**Figure 1.6:** Schematic view of the cathode: a) stick-type; b) button-type; c) cold cathode [23].

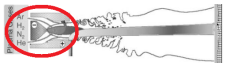

As it is presented in Figure 1.6, two configurations of the hot cathode are commonly used: the stick-type and the button-type cathode. The power levels of torches using the stick-type cathode range between 10 and 150 kW, with arc currents below 1000 A. The button-type cathode is cylindrical and characterized by the diameter almost equals the length. This kind of cathode is inserted partially or completely in a water-cooled copper holder. It is used mainly in transferred arc configuration with the arc current until 3-6 kA. The cold cathode is commonly made of the copper, silver or alloy. It has a very simple cylindrical shape with the cylinder closed at the one side. The cold cathode torches work with the power levels from about 100 W to 10 MW and the arc current levels in the range 100-3000 A.

- **Anode**

The anode is a passive component used to collect the electrons to obtain the current flow from the electrical circuit to the plasma. The anode-nozzle, at which the localized heat flux can reach 160 $W.mm^{-2}$, should be water-cooled and made of high purity oxygen free copper, characterized by high thermal conductivity: 358 $W.m^{-1}.K^{-1}$ and thermal diffusivity: 114 x $10^{-6}$ $m^2.s^{-1}$ at 25°C, often with an insert of sintered tungsten. Typical nozzle diameters are between 6 and 10 mm for arc currents between 300 and 1000 A. The anode nozzle design can highlight different process parameters, as a high gas velocity, narrower or wider temperature profiles, different arc length and arc voltages. It has been shown that a smaller nozzle diameter results in shorter arcs, lower temperatures at the nozzle exit, but also higher velocities for the same current and mass flow rate [24]. The anode configuration can be separated into two groups: the anode surface perpendicular and parallel to the plasma jet axis. The first configuration is used in the case of transferred arcs. The anode surface parallel to the jet axis is commonly found in the plasma torches.

- **Gas injection**

Three types of the gas injection are used in the plasma spraying method: the axial, radial and swirl injection, presented in Figure 1.7.

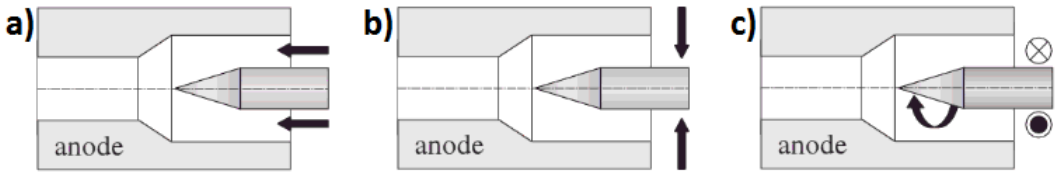


**Figure 1.7:** Schematic view of the gas injection: a) axial; b) radial; c) swirl [25].

In the axial injection the gas is injected parallel to the anode axis, Figure 1.7, and has the longitudinal velocity component. This type of the injection is mainly used in the torches with the stick-type cathode or the button-type for the high levels of the arc current (I > 1500A). In the case of the radial injection, the gas is injected perpendicular to the axis of the torch and presents strong radial component which afterwards is being reduced. In the swirl injection, the swirl flow creates the centrifugal forces, what pushes the cold gas towards the walls of the torch. The selection of the gas injection method has the influence on the arc current voltage, what was investigated in [26]. The use of the axial injector results in the longest arcs, the highest arc voltage, while the radial injection causes the shortest arc.

As has been mentioned, the plasma jet is produced by a torch in which the electrical arc is struck between a cathode, $\ominus$ in Figure 1.8, and an anode, $\oplus$. The arc column (3 in Figure 1.8) is developed from the cathode tip by pumping the part of the plasma forming gas (1), injected in the way described above.

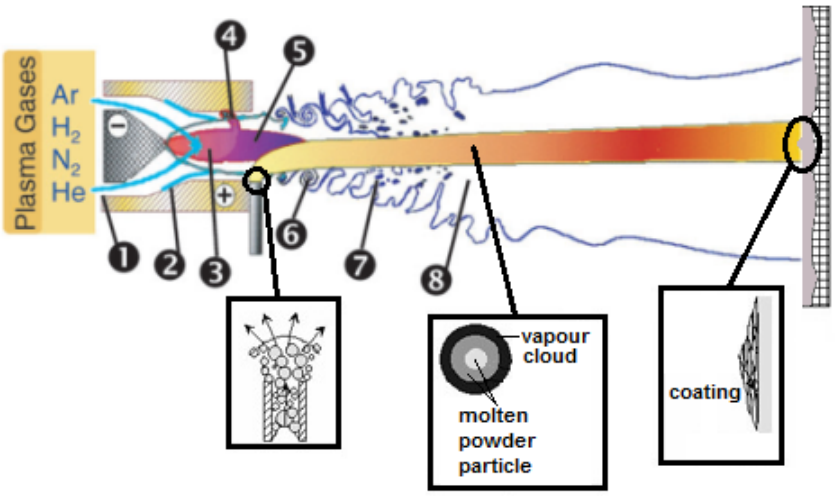


**Figure 1.8:** Schematic view of a plasma spraying method [15].

The arc column is characterized by a laminar flow which is limited by an isothermal envelope at $T = T_c$ (where $T_c$ is the critical temperature, defined in the section of Stationary behavior of the torch). Outside this area no electrical conduction is possible, which appears as a boundary between the arc column and the "cold" sheath (2 in Figure 1.8). Therefore, this column is constructed from the tip of the cathode to point on the anode wall, presented as (4) in 1.8. This arc attachment to the nozzle wall is perpendicular to the anode surface and is in the form of a high-temperature, low-density gas column cutting through the cold gas boundary layer. The thickness of this layer depends strongly on the plasma process parameters: the arc current, nozzle internal diameter, injection of plasma forming gases. The studies of the arc attachment to the anode wall have shown

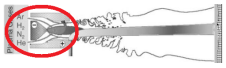

that it continuously fluctuates in length and position [27, 28]. This is due to the axial and rotational movements induced by the drag forces exerted by the cold flow in the boundary layer and the Lorentz forces. The rotational movement of the arc attachment is strongly favored by the swirl injection of the plasma forming gas. The axial displacement of the arc root gives the variation in the length of the arc column and, therefore, in enthalpy. The rotational displacement results in a nonsymmetry in the gas flow field and, consequently, inhomogeneity in the plasma jet. While the plasma jet, characterized by low density (approximately 1/30 of that of the cold gas) and a high speed (between 600 and 2200 m/s), exits the torch nozzle, it meets the surrounding atmosphere, what results in creating the swirl rings. They coalesce and cause large scale eddies (6 in Figure 1.8) which introduce cold surrounding gas bubbles (7).

#### 1.2.1.1 Characteristic of the plasma jet

The plasma is a complex mixture of gases, chemically neutral in order to reduce the erosion of electrodes. Typical plasma forming gases are argon (Ar), hydrogen ($H_2$), helium (He) and nitrogen ($N_2$). The choice of the injected gas plays a significant role in the plasma spraying technique. It defines important plasma thermodynamic and transport properties. The following paragraph is focused on the determination of these characteristics by the choice of the plasma forming gas. Firstly, the plasma state and laws describing this state of matter are given.

##### 1.2.1.1.1 Plasma state

The plasma in the plasma spraying method is obtained by the electric discharge produced by the direct current torch. The energy from the applied discharge is supplied to the plasma forming gas. If this energy is sufficiently high, it results in: the dissociation of molecules ($X_2 \longrightarrow 2X$) in case of molecular gases and the ionization of atoms ($X \longrightarrow X^+ + e$), where X symbolizes particular gas. Boulos *et al.* have summarized the energies of the main plasma forming gases, presented in Table 1.1.

**Table 1.1:** Ionization and dissociation energies of the plasma forming gases [17].

| Species | Ar | He | H | N | $H_2$ | $N_2$ |
|---|---|---|---|---|---|---|
| Ionization energy(eV) | 15.755 | 24.481 | 13.659 | 14.534 | 15.426 | 15.58 |
| Dissociation energy(eV) | - | - | - | - | 4.588 | 9.756 |

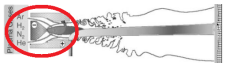

To sustain the plasma in thermal spray processes a relatively small degree of ionization of the gas is required (less than 1-3%). The degree of ionization is defined as follows:

$$\alpha = \frac{n_i}{n_n + n_i} \simeq \frac{n_i}{n_n} \tag{1.2}$$

where:

$n_i$ is the number density of ionized atoms,

$n_n$ the number density of neutral atoms.

In plasma systems, complete thermodynamic equilibrium (CTE) is related to uniform homogeneous plasma, in which kinetic and chemical equilibra are unambiguous functions of temperature. This temperature is supposed to be homogeneous and the same for all degrees of freedom, all the plasma system components, and all their possible reactions. Therefore, the following conditions should be fulfilled:

- The plasma is isotropic: the particles do not favor any direction of propagation. The velocity distribution functions for particles of every species must follow a Maxwell distribution as follows:

$$\frac{dn}{n} = \Big(\frac{m}{2\pi k_B T}\Big)^{3/2} exp\Big[-\frac{mv^2}{2k_B T}\Big] 4\pi v^2 dv \tag{1.3}$$

  where $m$ is the mass of the particle and $n$ the total number of particles.

- The population density of the excited states of every species follows a Boltzmann distribution:

$$\frac{n_j}{n} = \frac{g_j}{Q^{int}} exp\Big[-\frac{E_j}{k_B T}\Big] \tag{1.4}$$

  where:

  $n_j, g_j, E_j$ are respectively the density of population, the statistical weight and energy associated with the level j,

  $Q^{int}$ the partition function of the particular species, defined as follows: $Q^{int} = \sum_i g_i exp\Big[-\frac{E_i}{k_B T}\Big]$.

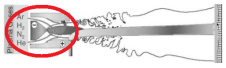

- The ionization equilibrium is described by the Saha equation:

$$\frac{n_e n_i}{n_0} = \frac{2{Q_i}^{int}}{{Q_0}^{int}}\left[\frac{2\pi k_B T m_e}{h^2}\right]^{3/2} exp\left(-\frac{E_i - \Delta E}{k_B T}\right) \tag{1.5}$$

where:

| | |
|---|---|
| $n_e, n_i, n_0$ | are the densities of electrons, the charged and neutral species, |
| ${Q_i}^{int}, {Q_0}^{int}$ | the partition functions of ionized atoms with the factor 2 corresponded to the statistical weight of the electron, |
| $E_i$ | the ionization energy of the gas, |
| $\Delta E$ | the correction due to the decrease of $E_i$ by electric-field effects. |

Moreover, the law of mass action of Guldberg-Waage, describing the molecular dissociation, should be also introduced:

$$\frac{n_a n_b}{n_{ab}} = \frac{{Q_a}^{int}{Q_b}^{int}}{{Q_{ab}}^{int}}\left[\frac{2\pi k_B T M_a M_b}{(M_a + M_b)h^2}\right]^{3/2} exp\left(-\frac{D_{ab}}{k_B T}\right) \tag{1.6}$$

where:

| | |
|---|---|
| $n_a, n_b, n_{ab}$ | are respectively the densities of the species: a, b and ab, |
| $D_{ab}$ | the dissociation energy of the molecule ab. |

- The electromagnetic radiation field is that of blackbody radiation of intensity, what is given by the Planck function:

$${L_\lambda}^0(T) = \frac{2hc^2}{\lambda^5}\left[exp\left(\frac{hc}{\lambda k_B T}\right) - 1\right]^{-1} \tag{1.7}$$

However, the plasma in CTE conditions cannot be practically produced in the laboratory. Most plasmas are optically thin over a wide range of wavelengths and, therefore, the plasma radiation is much less than that of a blackbody. Consequently, the plasma produced by e.g. dc torch is considered in more realistic approximation, so-called local thermodynamic equilibrium (LTE).

According to the LTE approach, a thermal plasma is considered as optically thin and thus does not require a radiation field that corresponds to the blackbody radiation, what means that the Planck's law is no longer valid. However, the collisional processes are required to be locally in equilibrium. Therefore, the populations of all species and their excited levels are described by the presented above equations of Maxwell, Boltzmann, Saha and Guldberg-Waage, but with a temperature, which can differ from point to point in space and time.

Consequently, the plasma can be considered in the local thermodynamic equilibrium when the following conditions are fulfilled:

- The different species of the plasma have a Maxwellian distribution
- The plasma is in the kinetic equilibrium. The ratio E/p (where E is the energy that electron receives, p is the pressure) is sufficiently small that the temperatures of electrons, $T_e$, and heavy particles, $T_h$, approach each other $T_e = T_h$, what is presented in Figure 1.9.

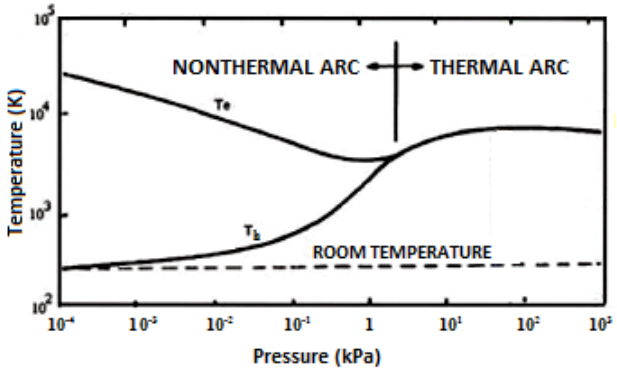


**Figure 1.9:** Evolution of electron temperature ($T_e$) and heavy particle temperature ($T_h$) in a mercury arc plasma [29].

- The collisions are the dominating mechanism for excitation (Boltzmann distribution) and ionization (Saha equilibrium).
- The spatial variations of the plasma properties are sufficiently small to give the chemical equilibrium.

However, it has been highlighted [17, 29, 30] that the equilibrium can be reached in the plasma core, not in the plasma boundaries, due to fast diffusion of electrons, and close to the walls or electrodes, where is a lower amount of the collisions.

#### 1.2.1.1.2 Thermodynamic and transport properties

The choice of the injected gas plays a significant role in the plasma spraying technique. It defines important plasma thermodynamic and transport properties: the specific enthalpy, electrical conductivity, viscosity, thermal conductivity, which will be described in the following paragraph.

The total enthalpy of the gas for high-velocity flows, $h_0$, has two components: kinetic enthalpy and static enthalpy related to the internal energy. The specific enthalpy is determined by the following equation:

$$h_0 = h_g + \frac{v_g^2}{2} \tag{1.8}$$

where:

$v_g$ is the gas velocity,

$h_g$ the static enthalpy related to the internal energy, defined as following:

$$h_g - h_g^{ref} = \int_{T_{ref}}^{T} c_p(T)dT \tag{1.9}$$

where:

$h_g^{ref}$ is the total enthalpy at the reference state: T = 0 K, p = 1 atm,

$c_p$ the specific heat.

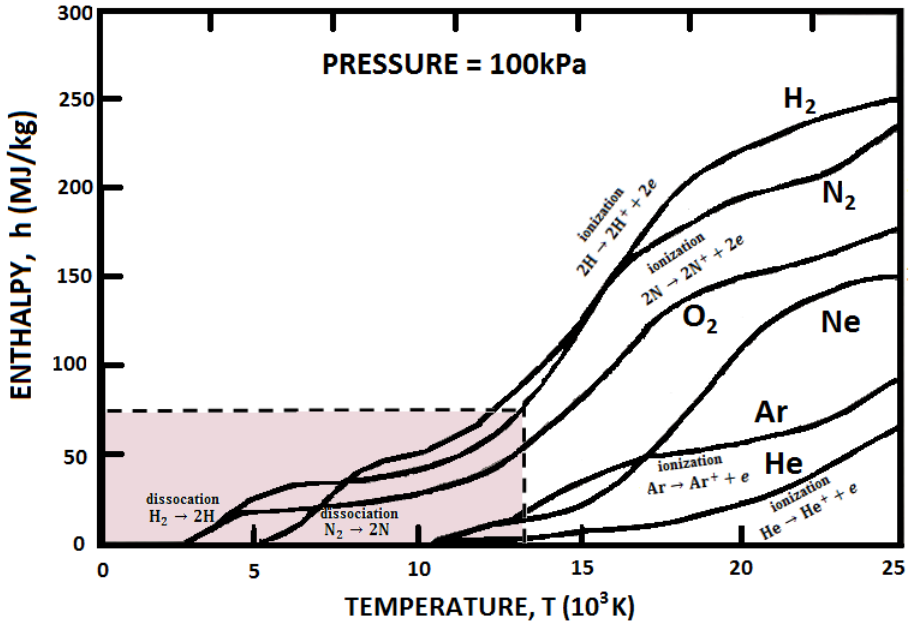


**Figure 1.10:** Specific enthalpy of various gases at atmospheric pressure with indicated region of interest [17].

Figure 1.10 shows the enthalpy of different plasma gases ($N_2$, $H_2$, Ar, He and $O_2$) as a function of temperature at atmospheric pressure. The plasma produced by dc plasma torch is characterized by the temperature up to 14 000 K, what has been indicated on the diagram. As can be noticed, the molecular gases have higher values of the enthalpy. The observed steep variations are caused by the heats of reaction (dissociation and ionization of the gas).

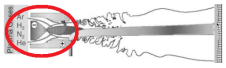

The use of argon provides high plasma temperature due to comparatively low enthalpy. The thermal expansion and thus high pressure lead to high plasma velocity. Adding helium further increases the velocity of the plasma. Therefore, argon/helium plasma is often referred to as cold and fast-moving whereas nitrogen/hydrogen is referred to as hot plasma.
In the plasma, the electrons and ions drift under the influence of an applied electric field, E, what gives rise to the density of the electric current, j, and can be presented by Ohm's law:

$$\vec{j} = \sigma_e \vec{E} \tag{1.10}$$

where:
$\sigma_e$ is the electrical conductivity, which can be defined by the following equation after applying the simplifications for the ions ($n_i = n_e$ and $\mu_i \ll \mu_e$):

$$\sigma_e = e.n_e.\mu_e \tag{1.11}$$

where:

| | |
|---|---|
| $e$ | is the electron charge ($1.6 \times 10^{-19}$ C), |
| $n_e$ | the electron density, |
| $\mu_e$ | the electron mobility. |

As it is presented in Figure 1.11 the values of the electrical conductivity for Ar, $H_2$ and $N_2$ are close, within the temperature difference of 1000 K, what can be explained by the similar values of the ionization energies of these gases, noted in Table 1.1.

For helium the difference of the electrical conductivity is more significant. The temperature values are shifted by around 5000 K due to higher ionization energy.

The viscosity, $\mu$, demonstrates the balance between the friction force in the direction of the plasma flow and the velocity gradient in the orthogonal direction. The dependence of $\mu$ on the temperature for different gases is presented in Figure 1.12. The drop of viscosity for temperatures above 10 000 K for Ar, $H_2$, $N_2$ and 17 000 K for He is due to ionization of the gas. When this process is significant the charged-species densities increase and their mobility decreases. Therefore, the molecular viscosity of thermal plasmas reaches its maximum when the volume fraction of the electrons reaches about 3%.

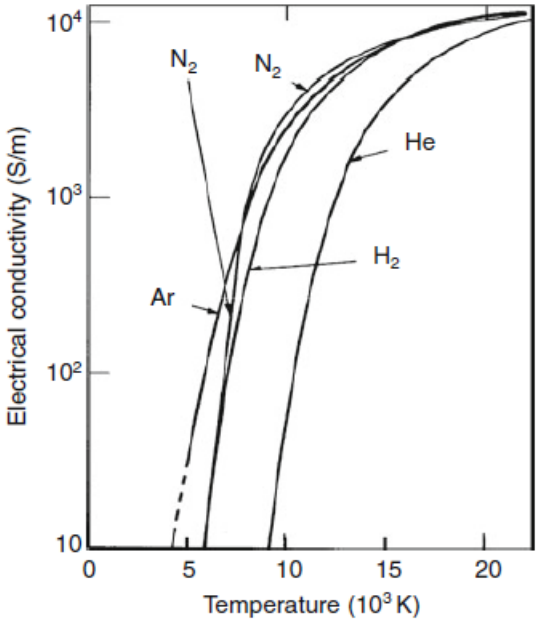


**Figure 1.11:** Dependence on the temperature of electrical conductivity of various gases [31].

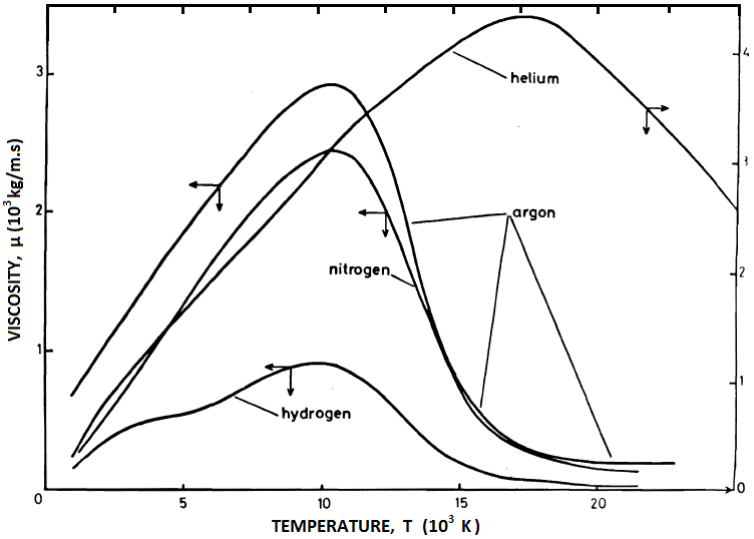


**Figure 1.12:** Temperature dependence of the viscosity of various gases ($H_2$, $N_2$, Ar, He) at atmospheric pressure [31].

As can be assumed from Figure 1.12 by adding helium to argon (He less than 60 vol.%) the viscosity keeps increasing up to 15 000 K instead of 10 000 K characteristic for argon. Then, it starts to decrease due to helium ionization. It permits to run slightly longer Ar-He jet than this obtained with Ar-$H_2$ mixture. Moreover, while mixing hydrogen with argon ($H_2$ less than 30 vol.%) the viscosity of argon is only slightly reduced as well as in case of $N_2$-$H_2$ mixture.

The thermal conductivity, $\kappa$, is one of the most important parameters of the thermal plasmas, which controls the energy losses in the arc as well as the heat transfer to sprayed particles. The thermal conductivity can be presented as the sum of three terms: $\kappa = \kappa_{tr} + \kappa_R + \kappa_{int}$, where $\kappa_{tr}$ results from the translation of species and is divided into: $\kappa_{tr}^h$ and $\kappa_{tr}^e$. The first element corresponds to the translational thermal conductivity of heavy species. The second, $\kappa_{tr}^e$, is the translational thermal conductivity of electrons, which becomes important above 8,000 K. $\kappa_R$, reactional thermal conductivity, results from the chemical reactions (dissociations, ionizations) and $\kappa_{int}$, internal thermal conductivity, from the internal degrees of freedom.
The temperature dependence of the thermal conductivity of the mixtures of argon with light gases is illustrated in Figure 1.13.

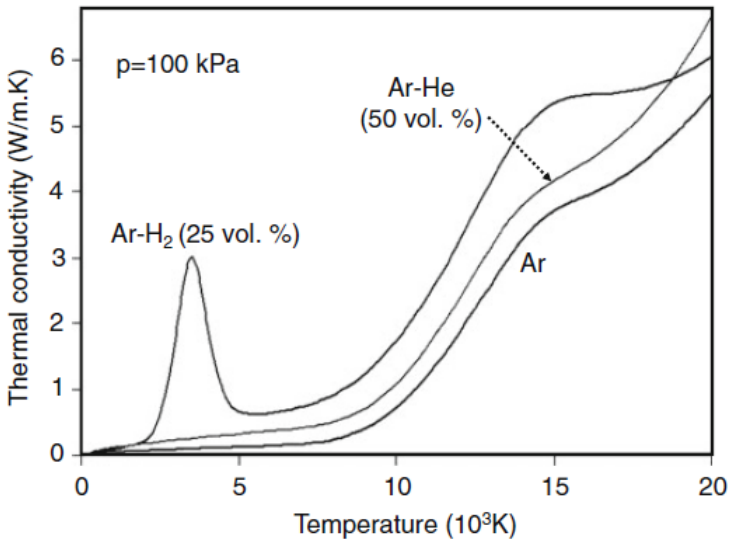


**Figure 1.13:** Temperature dependence of the thermal conductivity of the mixtures: Ar-H2 (25 vol.%), Ar-He (50 vol.%), and Ar at atmospheric pressure [17].

The mixture Ar-$H_2$ (25 vol.%) is characterized by the highest value of the thermal conductivity with the strong dissociation peak between about 2 500 and 5 000 K. The addition of helium to argon (He 50 vol.%) increases the thermal conductivity more regularly, what results in the values between these ones of argon and the argon-hydrogen mixture.
As has been presented, the plasma forming gases are characterized by different properties. Therefore, the mixtures of monatomic and molecular gases are often used in plasma spraying process [15, 23, 32].

### 1.2.2 Material injection

The plasma spraying is the method in which the molten material, by the plasma jet, is deposited on the substrate to form the coating. The previous part has presented the central part of this technique, the dc torch which converts the supplied energy into the stream of plasma. To obtain the coating the material has to be injected, heated and accelerated by the plasma jet toward a substrate. Therefore, the following section is focused on the material injection methods, what represents the second phase of the plasma spraying, indicated in Figure 1.3. Firstly, the technique used in the conventional APS method will be described. Than, the injection of the suspension droplets and the thermo-physical phenomena associated with this process will be presented.

#### 1.2.2.1 Material injection in conventional plasma spraying

In the conventional plasma spraying method (APS) the powders with the diameters typically between 10 $\mu$m and 110 $\mu$m are injected to the plasma jet. The material injection is performed mainly by a straight tube with an internal diameter in the range of 1.5 - 2 mm. Powder particles are carried by the gas, e.g. argon, with the flow rate in the range of 3 to 10 slm. In the case of conventional dc plasma torches the material is introduced to the plasma jet radially. The axial injection is performed in new designs of the torch, e.g. Axial III which will be presented in next sections.

#### 1.2.2.2 Suspension injection

As has been mentioned before, the following thesis is focused on the studies of dc plasma torch associated with the suspension injection. The suspension is formulated by the dispersion of fine powder particles within a solvent with the components which are added in order to improve the rheological properties, decreasing the agglomeration of fine solids and slowing down their sedimentation. The following section presents the suspension preparation process and different methods of the suspension injection.

##### 1.2.2.2.1 Suspension preparation

The suspension suitable for SPS process generally consists of the solid submicron or nanosized powder, the solvent and chemical additives. The first mentioned component of the suspension is the powder. The chemical components, size of particles, technology used in production are very important factors in the powder fabrication. The powders are

mainly produced by the chemical precipitation processes, mechanical crushing, milling, thermal treatments. The choice of the solvent is very important for the liquid feedstock properties such as low viscosity and good stability. Table 1.2 presents the parameters of main liquids used in the suspension: water and ethanol.

**Table 1.2:** The parameters of the most common solvents for the suspension preparation [33].

| Liquid | Surface tension | Viscosity | Specific heat | Latent heat of vaporization | Vaporization temperature |
|---|---|---|---|---|---|
| | $\sigma_s$ ($J.m^{-2}$) | $\mu_s$ (Pa.s) | $c_p$ ($J.kg^{-1}.\kappa^{-1}$) | $L_V$ ($J.kg^{-1}$) | $T_V$ (K) |
| Water | $72 \times 10^{-3}$ | $10^{-3}$ | $4.18 \times 10^3$ | $2.26 \times 10^6$ | 373 |
| Ethanol | $22 \times 10^{-3}$ | $1.06 \times 10^{-3}$ | $2.44 \times 10^3$ | $0.84 \times 10^6$ | 351 |

Comparing the properties of these two liquids it can be stated that water requires more energy than ethanol to get vaporized. In addition, ethanol is characterized by a lower surface tension. Nevertheless, it contains carbon which can pollute the coatings. Therefore, the mixture of the ethanol with water are commonly used.
A typical suspension preparation process is outlined in Figure 1.14.

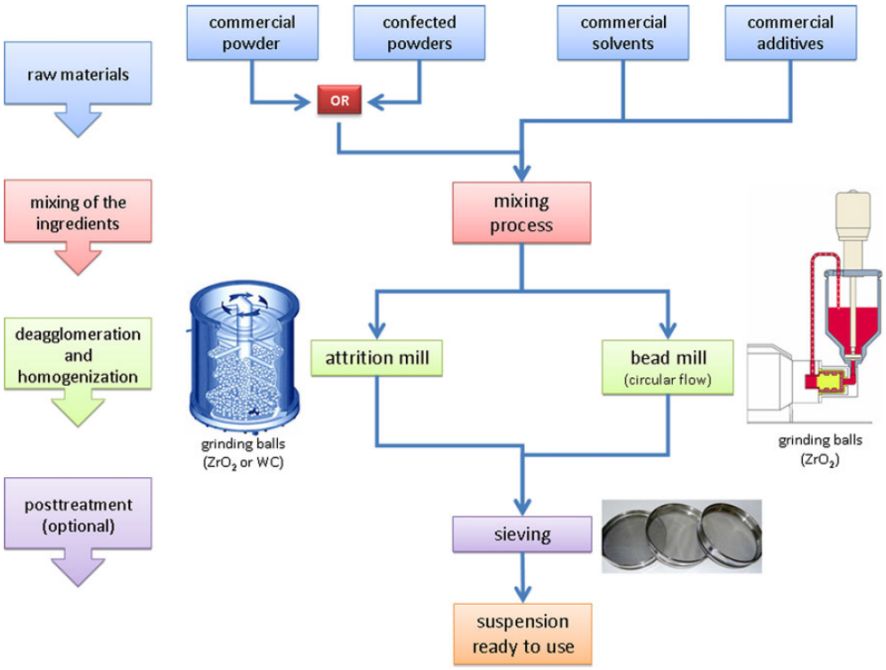


**Figure 1.14:** General preparation route for the suspension [34].

The most common way to produce the suspension is to make a simple slurry with powder particles and a solvent. To obtain good homogenization and deagglomeration of the suspension the slurry is treated by the attrition or bead milling. However, this process can be not sufficient for the nano-sized particles, especially of oxides which have the

tendency to agglomerate or aggregate. As shown in Figure 1.14 the dispersant is being added to the liquid feedstock to stabilize the powder within the solvent, e.g. a phosphate ester mixed with zirconia particles in [35]. It adsorbs on the particle surface and allows an effective dispersion of particles by electrostatic, steric, or electro-steric repulsions. By adding some supplements, e.g. ammonium polyacrylic acid (PAA) or polyvinyl alcohol (PVA), to the liquid feedstock is possible to modify the surface tension or the viscosity of the suspension. Good adjustment of these properties is important for the material injection and the treatment of the suspension droplets by the plasma, what is outlined in the following sections.

#### 1.2.2.2.2 Suspension injection methods

In suspension plasma spraying the liquid material is injected to the plasma jet by an adequate method. In the conventional systems the injection is carried out mainly by the atomization and mechanical injection. The following chapter describes these conventional methods. Moreover, new techniques, which enable to control the injection moment, will be presented.

##### 1.2.2.2.2.1 Spray atomization

This method uses an external energy, the atomizing gas, to break up the liquid into droplets. The low velocity liquid is injected inside a nozzle where is fragmented by a gas (mostly Ar because of a high mass density, presented in e.g. [36]) expanding within the body of the nozzle. Fauchais *et al.* have defined the types of break-up mechanisms due to the liquid viscosity, $\mu_l$ [37, 38]. The liquids with the viscosity between 0.1 and 50-60 mPa.s break-up into drops according to the Weber number, $We$, which is the ratio of the force exerted by the flow on the liquid to the surface tension force, defined as following:

$$We = \frac{\rho_g . v_r^2 . d_l}{\sigma_l} \tag{1.12}$$

where:

| | |
|---|---|
| $\rho_g$ | is the gas mass density, |
| $v_r$ | the relative velocity between the gas and the liquid, |
| $d_l$ | the diameter of the liquid droplet, |
| $\sigma_l$ | the surface tension of the liquid. |

For a fluid with higher viscosity the Ohnesorge number, $Oh$, has to be also considered. It relates the viscous forces to inertial and surface tension forces, according to the equation:

$$Oh = \frac{\mu_l}{\sqrt{\rho_g . d_l . \sigma_l}} \tag{1.13}$$

The typical sizes of atomized material droplets range between 2 and 100 $\mu$m, the corresponding velocities varying from 5 to 60 m/s.
There are many types of atomizers. One of the most widely used, the pneumatic droplets generator, is presented in Figure 1.15. It consists of a robust steel chamber, a nozzle at the bottom and a T-junction arrangement at the top.

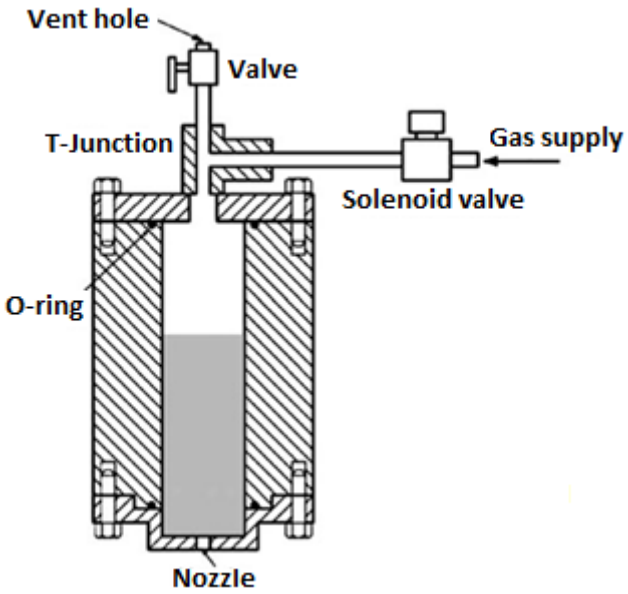


**Figure 1.15:** Schematic of a pneumatic droplet generator [39].

The functioning of pneumatic droplet generator based on applying pulses of a pressurized gas to the liquid contained in the chamber. The gas pulse forces out droplets through the nozzle in the bottom plate of the generator. A solenoid valve is rapidly opened and closed to create pressure pulses. In each pulse, one or more droplets emerge from the nozzle exit. The nozzle is a cylindrical synthetic sapphire nozzle of about 0,1 mm diameter. Due to this small size, droplets only may be ejected if a gas pressure pulse is applied. Droplet generation in this technique is controlled by the gas pulse duration (solenoid valve duration), the vent hole diameter and the gas supply pressure. In rotary atomizers centrifugal forces are used to further enhance the breakup process [40,41]. In this case the liquid is supplied to the centre of a spinning disk and liquid sheets or ligaments are thrown off the edges of the disk. Other types include vibratory and ultrasonic atomizers (or nebulizers), where the drops are formed by vibrating the injector nozzle at high frequencies and at large amplitudes to produce short-wave length disturbances to the liquid flow.

Ultrasonic atomizers are used in the applications where very fine sprays (submicron sizes) are required. The electrostatic atomizers can be also used for the generation of the droplets. In this type of atomizer the spray liquid is charged by applying a high-voltage drop across the nozzle. The dispersion of the spray drops is increased by exploiting electrical repulsive forces between the droplets.

#### 1.2.2.2.2.2 Mechanical injection

In the mechanical injection, shown in Figure 1.16, the suspension is stored in the pressurized tank from where it is forced through a nozzle of specified internal diameter, $d_n$ [33, 42–44]. Fazilleau *et al.* have used a calibrated nozzle hole with the diameter of 150 $\mu$m fabricated by the electro-erosion [43] and Etchart-Salas *et al.* have presented the results obtained by a laser-machined nozzle of diameter varying from 50 to 300 $\mu$m [33,44].

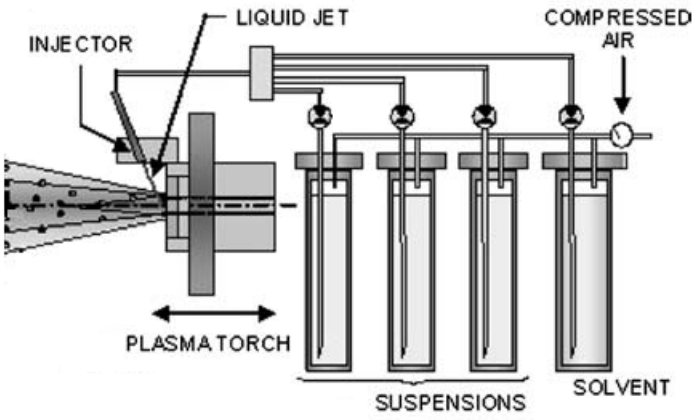


**Figure 1.16:** Schematic view of a mechanical injection [43].

The size of the droplets depends on the internal nozzle diameter following the relation: $d_l \simeq 1.9 \times d_n$ [45]. The suspension injection, in the mechanical method, is controlled by the pressure of the liquid in the reservoir. The mass flow rate, $\dot{m}_l$, is determined by the following equation:

$$\dot{m}_l = \rho_l . v_l . S_n \tag{1.14}$$

where:

| | |
|---|---|
| $\rho_l$ | represents the liquid specific mass, |
| $v_l$ | the liquid average velocity at the nozzle exit, |
| $S_n$ | the cross section area of the nozzle hole. |

The gas pressure difference, $\Delta p$, between the pressure in the container and the surrounding atmosphere is depicted by the equation:

$$\Delta p = \frac{f.\rho_l.v_l^2}{2} \tag{1.15}$$

where:

$f$ is the friction coefficient of the liquid in the injection nozzle which depends on nozzle

Fazilleau *et al.* have shown that the square of the liquid velocity varies linearly with the pressure of the reservoir. For example, injection velocities between 25 and 35 m/s were obtained with a tank pressure between 0.2 and 0.6 MPa.

#### 1.2.2.2.2.3 Alternative suspension injection methods

New methods have been developed to control the properties of the liquid injection. Blazdell *et al.* have highlighted the possibility of continuous suspension injection by superimposing a modulation signal to piezoceramic material of dc jet printer head (Domino Inkjet, Japan), presented in Figure 1.17 [46]. The liquid was forced through a 50 $\mu$m diameter nozzle under pressure (up to 0.5 MPa), superimposed by a piezoelectric drive rod modulated with frequency of 64 kHz. Using this operating frequency permits to produce 64000 drops per second.

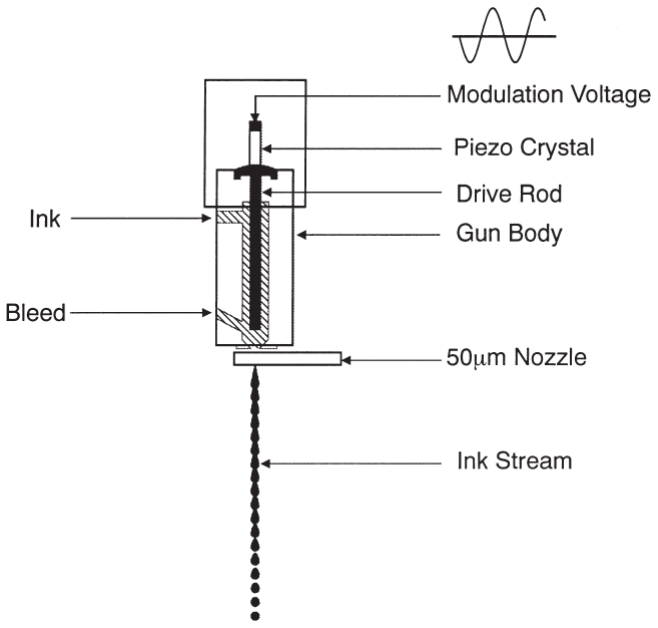


**Figure 1.17:** Schematic view of a jet printer head [46].

The drop diameter, $d_l$, depends on the factors, presented by the following equation:

$$d_l = \left[\frac{3d_n^2.v_l}{2f}\right]^{1/3} \tag{1.16}$$

where:

| | |
|---|---|
| $d_n$ | is the nozzle orifice diameter, |
| $v_l$ | the stream velocity, |
| $f$ | the frequency of piezoelectric modulation. |

The equation above shows that the drop diameter is a function of the liquid flow velocity and therefore these two important parameters can not be controlled separately. Oberste Berghaus *et al.* have described the similar method using a magnetostrictive drive rod (Etrema AU-010, Ames, Iowa) [47]. The suspension was injected from the pressurized reservoir through the nozzle with diameters varied between 100 and 255 $\mu$m. A magnetostrictive drive rod, mounted at the nozzle, applied the pressure pulses at different frequencies up to 30 kHz. This new injection method allowed producing 400 $\mu$m drops with 10 $\mu$s delay between each and with a velocity of 20 m/s.
Both methods permit to control the droplet diameter, flow rate and velocity. By superimposing signal to the injection head the uniformly spaced, suspension droplets can be generated.

#### 1.2.2.2.3 Thermo-physical phenomena of the droplets

The coatings obtained by the suspension plasma spraying method depend on the interaction between the plasma jet and the injected feedstock material. Therefore, understanding the movement and heating of the suspension droplets inside the plasma is the important part in the process. The study of the interactions between the liquid and the plasma jet should take into account the heat and momentum transfer to the particles, particle fragmentation and evaporation processes.

##### 1.2.2.2.3.1 Suspension penetration into the plasma jet

While the suspension jet or drops are injected to the plasma jet they are progressively or rapidly fragmented into droplets. It results in the decrease of their volume, what causes that the injection force of the droplets and force imparted to them by the gas jet are being decreased. Therefore, the droplets do not penetrate any more into the plasma jet.

Fazilleau has presented the condition for good suspension penetration into the plasma jet [35]:

$$\rho_l {v_l}^2 \gg \rho_p {v_p}^2 \tag{1.17}$$

where:

| | |
|---|---|
| $\rho_l$ | is the liquid density, |
| $\rho_p$ | the plasma mass density, |
| $v_l$ | the liquid velocity, |
| $v_p$ | the plasma velocity. |

Once the suspension droplets are entrained into plasma jet, they undergo the fragmentation process due to a strong shear stress (generated by the plasma flow) and the liquid vaporization caused by high plasma heat flux. The fragmentation depends on the dimensionless Weber number defined as follows:

$$We = \frac{{v_r}^2 . d_l . \rho_p}{\sigma_l} \tag{1.18}$$

where:

| | |
|---|---|
| $v_r$ | is the relative velocity between the gas and the liquid, |
| $d_l$ | the diameter of the droplet, |
| $\sigma_l$ | the surface tension of the liquid. |

Pilch and Erdman have determined the mechanisms of drop break-up according to We number, presented in Figure 1.18 [48].

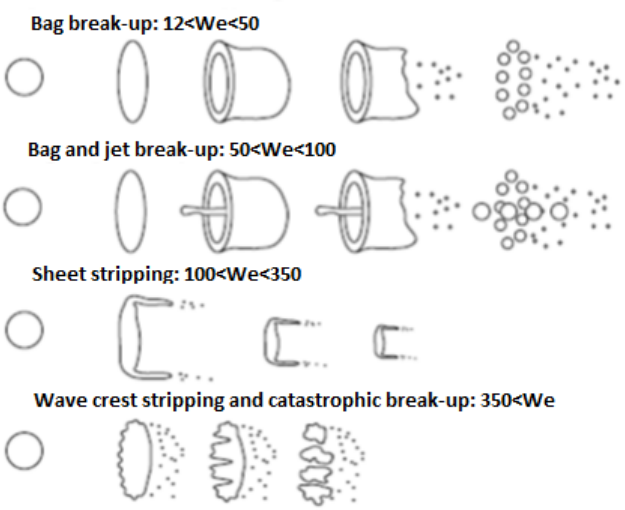


**Figure 1.18:** Droplet break-up mechanisms [48].

For $12 < We < 50$ and $50 < We < 100$ the fragmentation is called "bag break-up" and "bag and jet break-up" because it corresponds to the deformation of the drop as a bag-like structure. The droplet is stretched and swept off in the flow direction.
For $100 < We < 350$ the process is named "sheet stripping" fragmentation. Thin pieces of liquid are drawn from the periphery of the deforming droplets.
For $We > 350$ the fragmentation is called "wave crest stripping and catastrophic break-up" what corresponds to a multistage breaking process.
Moreover, the studies of the fragmentation process have shown that a Weber number of about 14 has been the critical value over which the droplet undergoes breakup. It has been highlighted by Basu *et al.* who have studied the phenomena associated with solution precursor plasma spray (SPPS) process [49, 50].
Once the suspension droplet is injected into the plasma it is exposed to the aerodynamic, $F_a$, and the surface tension, $F_s$, forces. The aerodynamic force of the plasma jet results in the break-up of the drop and the surface tension of the liquid opposes this force. To determine the minimum droplet diameter ($d_f$), when the fragmentation is completed, both forces are considered as following:

$$\frac{\pi}{8}.C_D.{d_f}^2.\rho.v^2 = \pi.d_f.\sigma \tag{1.19}$$

where:

| | |
|---|---|
| $C_D$ | is the flow drag coefficient, |
| $\rho$ | the plasma specific mass , |
| $v$ | the relative velocity between flow and drop, |
| $\sigma$ | the droplet surface tension. |

The minimum droplet diameter is then given by:

$$d_f = \frac{8.\sigma}{C_D.\rho.v^2} \tag{1.20}$$

The droplet diameter ($d_f$), when the fragmentation is completed, depends strongly on the liquid and the plasma flow velocity, what is shown in Table 1.3. The calculations of $d_f$ are presented for Ar-$H_2$ plasma jet.

**Table 1.3:** Calculation of fragmentation times for ethanol and water droplets for different plasma jet velocities [51].

| | v (m/s) | | |
|---|---|---|---|
| Calculation of $d_f$ ($\mu$s) | 500 | 1000 | 2000 |
| Water | 0.52 | 0.29 | 0.15 |
| Ethanol | 0.57 | 0.3 | 0.14 |

The important parameter of the fragmentation is the time duration of this process. Fazilleau *et al.* have shown that the fragmentation time, $t_f$, is given by [43]:

$$t_f = \frac{8\sigma(\frac{r_s}{r_d} - 1)}{C_D.\rho.v^3} \tag{1.21}$$

The model presented by Fazilleau considers that the radius of the initial droplet ($r_s$) is fragmented into n droplets of radius ($r_d$): $r_s{}^3 = n.r_d{}^3$.
All the droplets introduced into the plasma jet undergo heating resulting in solvent vaporization which is obtained by the energy balance equation:

$$4\pi.{r_s}^2.h_c(T - T_s) = L_V.\rho_s.\frac{dV_s}{dt} \tag{1.22}$$

where:

| | |
|---|---|
| $h_c$ | is the heat transfer coefficient, defined as follows: $h_c = \frac{\overline{\kappa}.Nu}{2r_s}$, |
| $T$ | the plasma temperature, |
| $T_s$ | the temperature at the surface of the liquid, |
| $L_v$ | the latent heat of the liquid vaporization, |
| $\frac{dV_s}{dt}$ | the volume variation of the droplet, determined as: $\frac{dV_s}{dt} = 4\pi {r_s}^2 \frac{dr_s}{dt}$. |

Assuming that during the vaporization time, $t_v$, the drop radius varies from $r_s$ to 0, $t_v$ is defined by the equation:

$$t_v = \frac{L_V.\rho_s.{r_s}^2}{(T - T_s)\kappa.Nu} \tag{1.23}$$

Figure 1.19 presents the comparison between the fragmentation and the vaporization times of ethanol droplet in the plasma jet (Ar-$H_2$, 45-15 slm, 500 A, anode nozzle diameter 7 mm).

It highlights that the fragmentation time is at least two orders of magnitude lower than the vaporization time. This difference is increased when the buffer effect of the vapour cloud around droplets is taken into account.

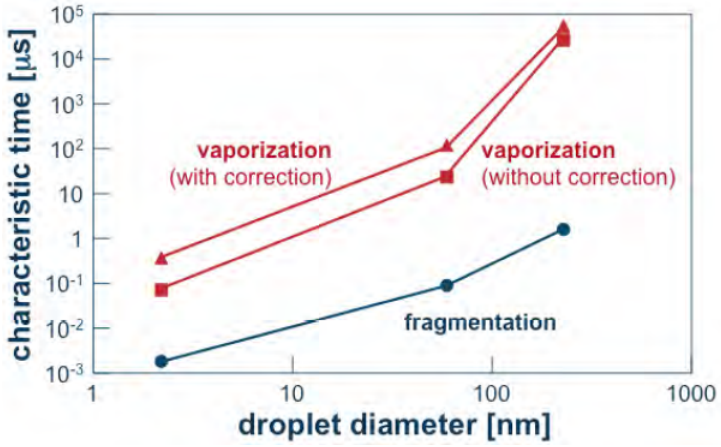


**Figure 1.19:** Variation of fragmentation and vaporization time of ethanol droplets inside Ar-$H_2$ plasma jet [43].

#### 1.2.2.2.3.2 Behaviour of the particle in plasma jet

The mechanism of the heat transfer from the plasma to the particle and the particle to the surroundings is presented in Figure 1.20.

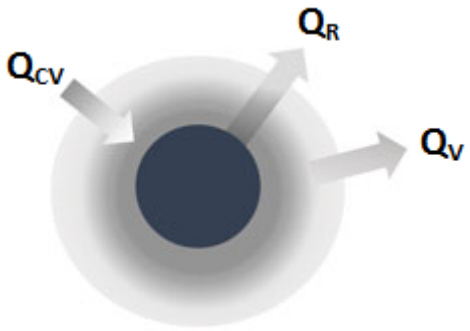


**Figure 1.20:** Schematic view of the heat transfer between the particle and the plasma [51].

The balance between conduction and convection heat ($Q_{CV}$) transfers from the hot gas to the particle and particle cooling due to radiative heat losses from the surface ($Q_R$) and losses from radiating vapour ($Q_V$) determines the net heat transfer to a particle ($Q_{net}$) by the following equation:

$$Q_{net} = Q_{CV} - Q_R - Q_V \tag{1.24}$$

The convection process has a major contribution to the heat transfer at the moment of the droplet injection to the plasma jet and at the end of particle flight if the gas become cooler and slower than the particle. The conduction is important when the relative velocity decreases, what corresponds to the middle of the particle flight. The radiative losses are significant when the temperature and size of the particles are relatively high.

Boulos *et al.* have shown that they affect the heat transfer in the case of pure argon plasmas when the heat transfer coefficient, $h_c$, is low [17].
The conduction and convection mechanisms are usually described by the Nusselt number:

$$Nu = \frac{h_c.d_l}{\kappa} = 2 + 0.6 \times Re^{0.5} \times Pr^{0.33} \tag{1.25}$$

where:

| | |
|---|---|
| $\kappa$ | is the thermal conductivity of the fluid, |
| $d_l$ | the liquid particle diameter, |
| $Re$ | Reynolds number, |
| $Pr$ | Prandtl number. |

The first term of the right-hand side of Equation (1.25) determines the conduction mechanism. It is dominant in the case of small values of Reynolds number, Re, defined as follows:

$$Re = \frac{v_r.d_l.\rho_g}{\eta_l} \tag{1.26}$$

where:

| | |
|---|---|
| $v_r$ | is the relative velocity between the gas and the liquid, |
| $\rho_g$ | the gas mass density, |
| $\eta_l$ | the liquid particle viscosity. |

The conduction mechanism is principal when i.e. the particle has a velocity nearly equal to the velocity of the gas. Such a case occurs when a particle is in the middle of its flight. Otherwise, the second term, the Prandtl number, must be considered, defined as:

$$Pr = \frac{c_{p_g}\eta_p}{\kappa} \tag{1.27}$$

In the case of nanometer and sub-micrometer sized particles of the suspension the Knudsen effect, which reduces the heat transfer, should be also considered. It depends on the Knudsen number defined as follows:

$$Kn = \lambda/d_p \tag{1.28}$$

where $\lambda$ defines the mean free path of the plasma molecules. It has been demonstrated that the Knudsen effect should be taken into account when the ratio of the plasma molecules mean free path, $\lambda$, to the particle diameter, $d_p$, is smaller than one ($0.1 < Kn < 1.0$) [17]. While the particle is moving in the plasma jet is exposed to a number of forces, which act

simultaneously on the particle and have varying influence on its trajectory and residence time in the plasma. The most important impact have inertia forces, $F_i$, and the viscous drag forces, $F_D$, defined as follows:

$$F_i = \frac{\pi {d_p}^3}{6}.\rho_p.\frac{dv_p}{dt} \tag{1.29}$$

$$F_D = \frac{\pi {d_p}^2}{4}.C_D.\frac{1}{2}.\rho_g.{v_r}^2 \tag{1.30}$$

As Pawlowski has presented, in most practical cases met in thermal spraying, only the drag force is taken into account and the force balance around a single particle in motion in a plasma flow can be written as: $F_i = F_D$ [42]. The drag coefficient, $C_D$, depends on the particle velocity relative to the flame velocity, what is determined by the Re number and presented in Table 1.4.

**Table 1.4:** Equations for $C_D$ of a single sphere according to the Re number [42,51].

| | |
|---|---|
| $C_D = \frac{24}{Re}$ | $Re < 0.2$ |
| $C_D = \frac{24}{Re}[1 + 0.187 \times Re]$ | $0.2 \leq Re < 2$ |
| $C_D = \frac{24}{Re}[1 + 0.11 \times Re^{0.81}]$ | $2 \leq Re < 20$ |
| $C_D = \frac{24}{Re}[1 + 0.189 \times Re^{0.62}]$ | $20 \leq Re < 200$ |

In the case of the particles below 0.1 $\mu$m the thermophoresis force should be taken into account in the areas characterized by the steep temperature gradients. The small particles change their trajectories from the plasma core to the jet fringes characterized by lower gas temperature and velocity. Moreover, because of their low inertia, the particles can follow the hot gas trajectory which flows parallel to the substrate surface and never impact on it. It occurs when the particles velocity is below: $St < 1$. St, the Stokes number, characterizes the behaviour of particles suspended in a fluid flow, as follows:

$$St = \frac{\rho_p {d_p}^2 v_p}{\mu_g \iota_{BL}} \tag{1.31}$$

where:

$\rho_p$ is the particle specific mass,
$\mu_g$ the gas viscosity,
$\iota_{BL}$ the thickness of the flow boundary layer, BL, in front of the substrate.

When $St > 1$, that is when particles velocity is high enough, particles can cross the boundary layer that develops at the substrate surface and impact on it.

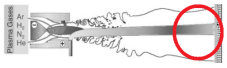

### 1.2.3 Coatings formation

The following section presents the last phase of the plasma spraying process- the material deposition.
Particles with given temperatures (above or close to their melting temperature) and velocities impact and flatten on the substrate, or previously deposited material, forming lamellae (splat). At impact with the substrate the particle flattens and the high pressure inside it forces melted material to flow laterally and ductile material to deform. The particle kinetic energy is transformed into work of viscous deformation and surface energy. The structure of the splat results from the spreading and solidification of the particles onto the substrate, what depends on the following parameters:

- the velocity and size of particle
- properties of the particle material in the liquid state, e.g. viscosity, surface tension
- ability of the wetting the substrate by liquid particles
- impact angle relative to the substrate
- surface roughness of substrate

The splat adhesion to the substrate depends strongly on the surface morphology of the base material. Therefore, the substrate has to be adequately prepared. The standard process is roughening of the surface by abrasive grit blasting. The substrate surface is blasted with compressed air jets carrying the abrasive grits, the angular particles of chilled cast iron or ceramic. In the plasma spraying process the stainless steel, aluminium or titanium substrates are commonly used. Therefore, the grits of 16-60 $\mu$m are generally applied. The preparation of the surface by abrasive grit blasting should answer the following purposes. Firstly, it should clean and activate the surface in order to avoid bonding defects in the interface between coating and base materials. The surface before this process can be treated by solvents, e.g. trichloroethylene, in order to remove the oil, grease or dirt. Secondly, grit blasting has to provide the right surface roughness to increase the effective surface area and to improve adhesive bonding of the sprayed deposit. The splat formation is presented in Figure 1.21. The flattening time is in the range of a few $\mu$s. The solidification process is longer though solidification starts before flattening is completed.

The time between two successive impacts is in the range of ten to a few tens of $\mu$s. Therefore, the next particle impacts on an already solidified splat.

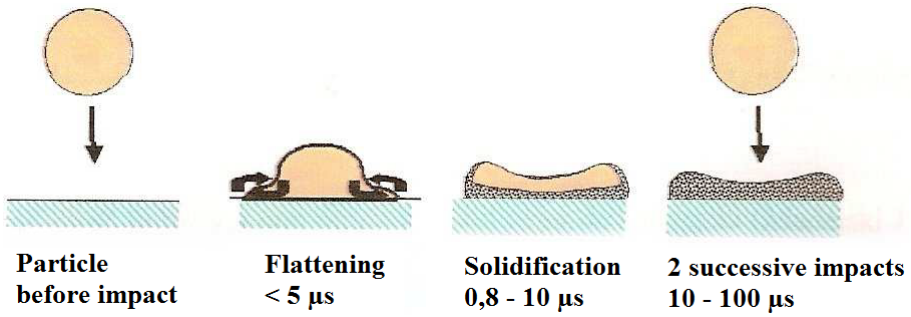


**Figure 1.21:** Characteristic time of lamallea formation in the conventional plasma spraying method [45].

The microstructure of the $Al_2O_3$ coating examined by a scanning electron microscopy (SEM) is presented in Figure 1.22. The suspension has been mechanically injected to the plasma jet produced by a stick-cathode dc plasma torch developed by Tingaud *et al.* [52, 53]. The torch has been operated with Ar-$H_2$ (45-15 slpm) plasma forming gas mixture and the arc current of 500 A.

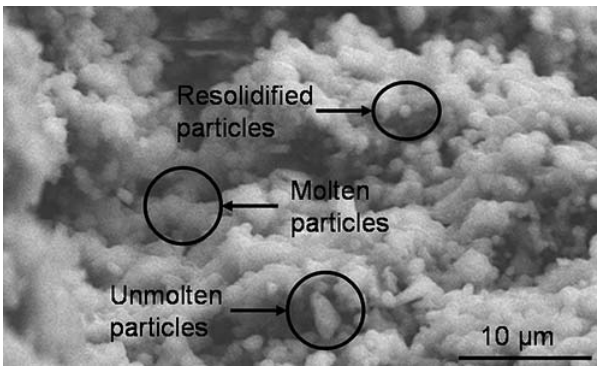


**Figure 1.22:** $Al_2O_3$ SPS coating architecture. Process parameters: Ar-$H_2$ 45-15 slpm, I = 500 A, h = 14 MJkg$^{-1}$, mechanical suspension injection, feedstock $d_{50}$ = 500 nm [53].

The examination of the coating has highlighted that it contains layered splats, unmolten particles (angular particles) and molten particles resoldified before their impact on the substrate (small spherical grains), what is highlighted in Figure 1.22.
To compare the results obtained by a stick-cathode dc plasma torch, the microstructure of the coating obtained by Triplex I plasma gun, described in the next section, is presented in Figure 1.23.

The coating microstructure consists of thin lamellas formed by single splats, which contain fine-grained, overspray particles (E) and re-solidified particles (C). The coating shows areas of good (A) and poor (B) inter-splat bonding. The splats have a columnar grain growth (D) with a grain thickness up to 0.1 $\mu$m. Moreover, the microstructure is characterized by inter-lamellar cracks (G), microcracks (H) and intrasplat cracks (F).

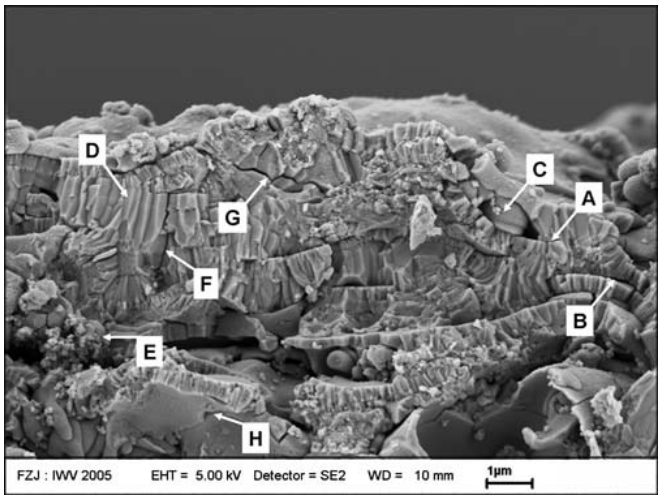


**Figure 1.23:** Main fracture features of 5YSZ SPS coating produced by Triplex I plasma gun [54].

Comparing both coatings microstructures, obtained by SPS method using the conventional torch and Triplex I plasma gun, it can be noticed that Triplex allows obtaining more and thinner lamellas formed by single splats. However, the similar features between two microstructures can be also found, e.g. the re-solidified or overspray particles. It can be assumed to the poorly controlled heat and momentum transfers between plasma and suspension, what is emphasized by the plasma fluctuations, presented in the following section.

## 1.3 Plasma instabilities

In the plasma spraying method most of the torches are supplied by a direct current (dc) power source. However, in spite of this fact, the plasma jet produced by a torch presents unsteady characteristics.

Etchart *et al.* has studied the suspension fragmentation process according to the arc voltage fluctuations, what is presented in Figure 1.24. The commercial dc plasma torch (PTF4 from Sultzer Metco) has been operated with Ar-$H_2$ (45-15 slpm) plasma forming gas mixture and the arc current of 503 A. The time-resolved imaging system permitted to observe the suspension penetration within chosen moments of the fluctuating plasma jet. Figure 1.24 shows the pictures taken for an instantaneous arc voltage of (a) 65 V and (b) 40 V. The differences in the droplets fragmentation and trajectory highlight the strong influence of the plasma jet fluctuations on the SPS method.
This time-fluctuating momentum of the plasma results in a poor reproducibility and reliability of the method, what causes the limited applications of suspension plasma spraying in advanced processing.

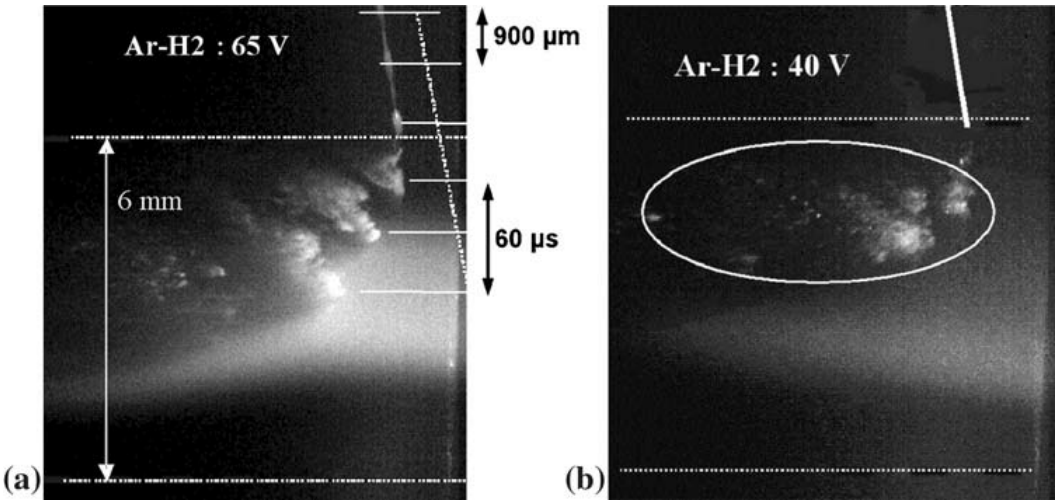


**Figure 1.24:** Plasma-suspension interaction at the triggering level of (a) 65 V and (b) 40 V [44].

Therefore, for many years, the special efforts have been devoted to understand the arc behavior in dc plasma torch, what is described in the following paragraphs.

### 1.3.1 Stationary behavior of the torch

To estimate the characteristics of the plasma jet and highlight the influence of experimental parameters on plasma jet velocity and pressure contributions, the simplified analytic model has been presented in [55]. The electrical conductivity and the heat potential have been presented in function of the specific enthalpy, what is highlighted in Figure 1.25.

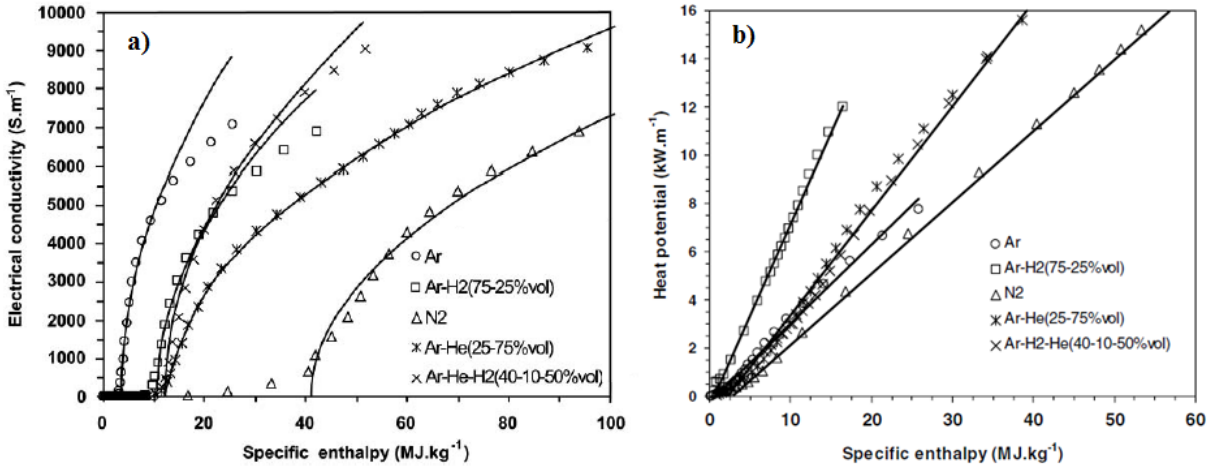


**Figure 1.25:** Dependence on specific enthalpy of: a) the electrical conductivity, b) the heat potential of various gases [55].

The representation of the electrical conductivity, given in Figure 1.25 a), allows defining the critical specific enthalpy, $h_c$ given in Table 1.5, which represents the electrical conduction threshold, the enthalpy value above which the electrical conduction begins. To define the threshold of electrical conduction in nitrogen, the electrical conductivity has been fitted by a basic square root function:

$$\sigma(h) = \partial_\sigma (h - h_c)^{0.5} \tag{1.32}$$

for $h \geqslant h_c = h(T_c)$

Figure 1.25 b) highlights the linear dependence on the specific enthalpy of the heat potential, in the range of interest of spraying application, defined by the Kirchoff's equation as follows:

$$\kappa(T) = \frac{d\varphi}{dT} \tag{1.33}$$

where: $\kappa$ and $T$ are, respectively, the thermal conductivity and the temperature. If $\overrightarrow{q}$ is the heat flux, the heat potential can be written as: $\overrightarrow{q} = -\overrightarrow{\nabla}\varphi$.

**Table 1.5:** Critical enthalpy, $h_c$, at the electrical conduction threshold, linear coefficient between heat potential and specific enthalpy, $a_\varphi$, and coefficient used for electrical conduction as a function of specific enthalpy, $\partial_\sigma$, for different plasma forming gases [55].

| Plasma gas | Ar | Ar-$H_2$ (75-25 vol%) | $N_2$ | Ar-He (25-75 vol%) | Ar-$H_2$-He (40-10-50 vol%) |
|---|---|---|---|---|---|
| $h_c$ ($MJ.kg^{-1}$) | 3.70 | 10.40 | 41.10 | 13.20 | 12.14 |
| $a_\varphi$ ($10^{-4}kg.m^{-1}.s^{-1}$) | 3.06 | 7.06 | 2.82 | 4.33 | 4.31 |
| $\partial_\sigma$ ($C.V^{-1}.m^{-2}$) | 1.89 | 1.42 | 0.95 | 1.03 | 1.56 |

The representation of the electrical conduction as the function of the specific enthalpy has leaded to estimate the plasma produced by a torch in the frame of a two-layer model, presented in Figure 1.26, if $h > h_c$ takes place.

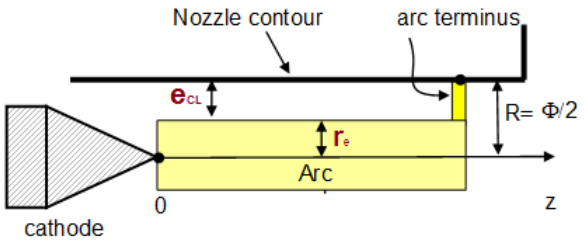


**Figure 1.26:** Schematic view of the two-layer model.

$e_{CL}$ represents the thickness of the cold layer where the electrical conductivity is neglected, outside $h_c$ surface. A mean radius, $r_e$, of the plasma is defined as follows: $h(r_e) = h_c$.

The main purpose of this model is to determine the enthalpy radius profiles to deduce the stationary characteristics of the plasma jet at the nozzle exit as function of easily measured experimental parameters (arc current, mean voltage, electrode thermal losses) and thermophysical properties of the plasma.
The specific enthalpy of the plasma results from the energy balance measurement of the electric power input, dissipated by Joule heating, and thermal losses due to radiation. The kinetic energy is negligible, therefore the energy equation is presented as follows:

$$\rho u \frac{\partial h}{\partial z} = \sigma E^2 + \nabla^2 \varphi - q_r \tag{1.34}$$

where $z$, $\rho$, $\sigma$, $E$, $q_r$ are, respectively, the axial coordinate, the plasma density, the electrical conductivity, the electric field and the radiative losses. By assuming that the density of mass flux is constant, introducing the term $s_h$ as the group of the convective specific enthalpy term, the Joule heating term and the radiative losses term, and by expressing the linearity between heat potential and specific enthalpy, the radial profile, h(r), at the nozzle exit can be deduced in the plasma ($0 \leq r \leq r_e$) and in $e_{CL}$ ($r_e \leq r \leq R$):

$$\frac{1}{r}\frac{\partial}{\partial r}\left(r\frac{\partial h}{\partial r}\right) = \frac{s_h}{a_\varphi} \tag{1.35}$$

what allows determining the simple parabolic profile of the specific enthalpy within the plasma and a logarithmic one within $e_{CL}$, as follows:
For the arc column ($0 < (R/r_e)^2 < 1$):

$$h = h_c + \Delta h\left[1 - \left(\frac{R}{r_e}\right)^2\right] \tag{1.36}$$

For the cold sheath ($(R/r_e)^2 > 1$):

$$h = h_c - h_e\left[1 - \left(\frac{R}{r_e}\right)^2\right] - (\Delta h + h_e) ln\left(\left(\frac{R}{r_e}\right)^2\right) \tag{1.37}$$

where: $\Delta h = |s_h|.r_e^2/4a_\varphi$. $\Delta h$ and $r_e$ have been determined from two conditions: one concerning the overall thermal balance and the other one, the gas enthalpy at the anode wall whose temperature is sufficiently low so that: $h(R) = 0$. The integration of equation (1.35) by using (1.36) and (1.37), and reduced variables: $x = \overline{h}/h_c$, $y = (r_e/R)^2$ gives:

$$x ln(y) = \frac{1}{2}y - 1 \tag{1.38}$$

what defines the overall thermal balance as non-dimensional variables and is solved by using a Newton-Raphson method.

The derivation of the boundary condition, h(R) = 0, in terms of x and y variables, allows determining: $\Delta h = -\frac{h_c}{\ln(y)}$ and $r_e = R\sqrt{y}$.
The presented model permits, by introducing a mean isentropic coefficient, to calculate the axial velocity of the plasma jet at the nozzle exit. The plasma flow at the nozzle exit is assumed to be equivalent to an isentropic fictitious plasma flow presenting the same stagnation properties. Following basic consideration of compressible fluid mechanics, the energy conservation is applied along a streamline crossing the nozzle exit section at a distance r from the nozzle axis. Using the Barré de Saint-Venant relationship for an isentropic and compressible flow, it can be written as follows:

$$\frac{1}{2}u^2(r) + \frac{\gamma}{\gamma-1}\frac{P_a}{\rho(r)} = h(r) \tag{1.39}$$

By using $\dot{m} = \rho u S$, where S is the area of the nozzle cross section, equation (1.39) becomes:

$$u^2(r) + \frac{2\gamma P_a S}{(\gamma-1)\dot{m}}u(r) - 2h(r) = 0 \tag{1.40}$$

what leads to simple formula for the plasma velocity:

$$u(r) = v^*\left(\sqrt{1 + \frac{2h(r)}{v^{*2}}} - 1\right) \tag{1.41}$$

where:

$$v^* = \frac{\gamma}{\gamma-1}\frac{P_a S}{\dot{m}} \tag{1.42}$$

In general $v^{*2} >> 2h(r)$, therefore, the above equation is written as $u(r) \simeq h(r)/v^*$ within 10% of accuracy. This relationship can be used to define an averaged velocity, $u_0$, by using the measured specific enthalpy $h_0$ as follows:

$$u_0 = h_0\frac{\dot{m}(\gamma-1)}{P_a S\gamma} \tag{1.43}$$

where $\gamma$ is the averaged isentropic exponent, directly linked to the plasma enthalpy or the ionization degree, what has been defined from an analysis of pressure contributions in the plasma flow, presented below. This obtained equation has been highlighted to be qualitatively in agreement with the relationship giving the maximum axial velocity of a nitrogen and an argon-hydrogen plasma jet deduced from measurements by Planche *et al.* as follows [24]:

$$u_{max} = K\frac{\dot{m}^{0.21}I^{0.44}}{R^{1.96}} \tag{1.44}$$

where K depends on the plasma gas chemical composition.

To find the pressure variations between the nozzle exit and a point located on the gas feeding line of the plasma torch, the total pressure has been measured as follows:

$$P_t = P_a + \Delta P_f + \Delta P_{is} + \Delta P_v + \Delta P_m \tag{1.45}$$

where:

$P_a$ is the atmospheric pressure,

$\Delta P_f$ the overpressure due to the cold gas flow between the measurement point in the gas feeding line and the arc region,

$\Delta P_m$ the magnetic overpressure at the cathode tip due to the Maecker effect

$\Delta P_{is}$ the isentropic overpressure which is the driving pressure, defined as follows: $\Delta P_{is} = \dfrac{h_0 \dot{m}^2 (\gamma - 1)}{2\gamma S^2 P_a}$,

$\Delta P_v$ the overpressure due to the plasma viscosity within the nozzle, admitted to be proportional to the nozzle length $\ell$, defined in two different ways:
1) as a linear loss pressure proportional to the nozzle length: $\Delta P_v = \dfrac{\alpha \ell}{2} \rho u^2$,
2) assuming a Poiseuille flow at the nozzle exit: $\Delta P_v = \dfrac{128 \overline{v} \dot{m} \ell}{\pi d^4}$.

The sum $(P_a + \Delta P_f)$ has been obtained as the results of the pressure measurements for the different mass flow rates and internal nozzle diameter without generating the plasma. If $\Delta \mathrm{P_p} = \mathrm{P_t} - (\mathrm{P_a} + \Delta \mathrm{P_f})$, $\Delta \mathrm{P_p}$ is defined as follows:

$$\Delta P_p = \Delta P_m + \left(\frac{\gamma - 1}{2\gamma}\right) \frac{\dot{m}^2 h_0}{S^2 P_a} (1 + \alpha \ell) \tag{1.46}$$

The equation leads to the linear relationship between the measured overpressure, $\Delta \mathrm{P_p}$, and the term $\dot{\mathrm{m}}^2 \mathrm{h_0}$ which is known from the experimental parameters, what is presented in Figure 1.27.

Figure 1.27 represents the dependence of the measured mean pressure on the term consisting of the mass flow rate of gases and the specific enthalpy, which is defined experimentally as follows: $\mathrm{h_0} = \dfrac{\mathrm{UI} - \mathrm{Q_{loss}}}{\dot{\mathrm{m}}}$, where U, I , and $\mathrm{Q_{loss}}$ are the measured mean values, respectively, of the arc voltage, of the arc current and of the torch thermal losses. Therefore, it can be assumed that these parameters influence $\Delta \mathrm{P_p}$, what has leaded to the studies presented in chapter 2.

To define the averaged isentropic exponent, $\gamma$, the Poiseuille flow is considered, and written as:

$$\Delta P_{is} = (\Delta P_p - \Delta P_m - \frac{128 \overline{v}}{\pi} \frac{\dot{m} \ell}{d^4}) = \left(\frac{\gamma - 1}{2\gamma}\right) \frac{16 h_0 \dot{m}^2}{P_a \pi^2 d^4} \tag{1.47}$$

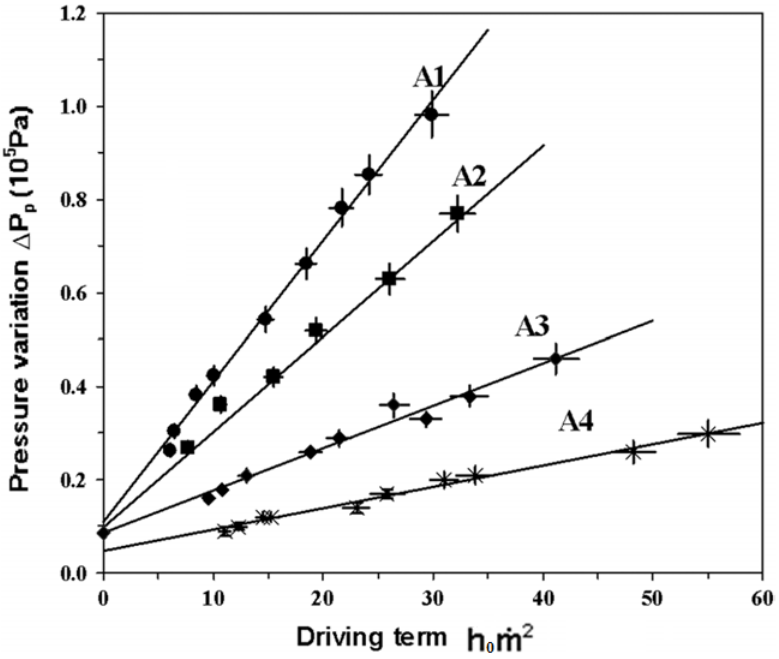


**Figure 1.27:** Pressure variation $\Delta P_p$ as function of $\dot{m}^2 h_0$ where $\dot{m}$ and $h_0$ are, respectively, the mass flow rates of gases and the specific enthalpy measured for the different anodes A1, A2, A3 and A4, the arc current from 350 to 600 A and plasma gas (Ar-$H_2$) mixtures: 30/10 45/15 60/30 (slm) [55].

Therefore, the isentropic component, $\gamma$, has been determined from the ratio $(\gamma - 1)/2\gamma$ defined as the slope of the evolution of $\Delta P_{is}$ as a function of $16 h_0 \dot{m}^2 / P_a \pi^2 d^4$ for the different experimental conditions, presented in Figure 1.28. As can be noticed the linear variation of the ratio $(\gamma - 1)/2\gamma$ has been obtained.

The presented results have been focused on the stationary behavior of the dc plasma torch. The plasma produced by a torch has been estimated in the frame of a two-layer model. It has permitted to determine the enthalpy radius profile to deduce the stationary characteristics of the plasma jet (at the torch exit) as a function of the measured parameters, e.g. arc current, mean voltage. It has leaded to calculate the axial velocity of the plasma jet at the nozzle exit and to evaluate the different pressure contributions. The determination of pressure as a function of the term $\dot{m}^2 h_0$ has shown the linear relationship between the mean pressure in the rear part of the plasma torch and the mean arc voltage, what has leaded to the studies of the pressure and the arc voltage presented later in this dissertation. The following paragraph will be focused on the studies of the arc instabilities and determination of different modes of these fluctuations.

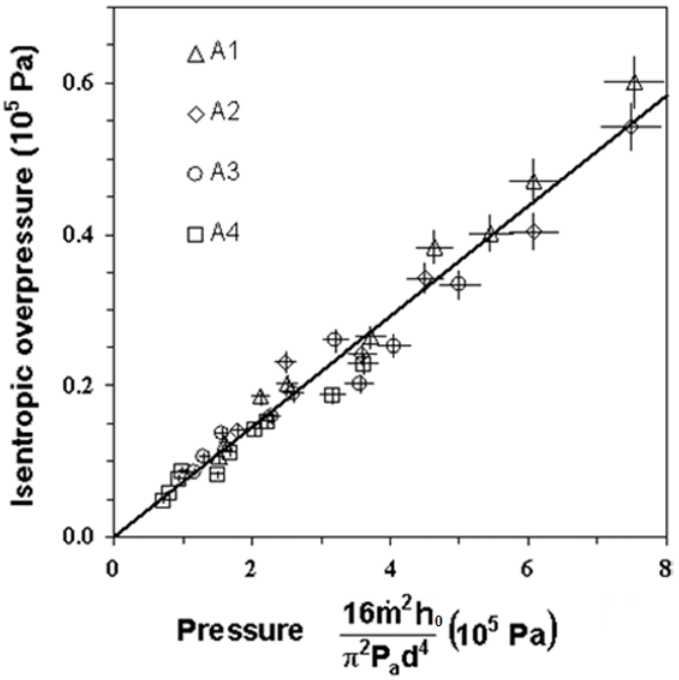


**Figure 1.28:** Dependence of isentropic pressure $\Delta P_{is}$ on experimental operating conditions [55].

### 1.3.2 Dynamic behavior of the torch: arc instabilities

The first experimental studies of the instabilities of electric arc with a superimposed flow of argon have been presented by Wutzke *et al.* [28]. The experiments have been performed in the arc tunnel by using a plane anode and the cathode positioned upstream, a double-anode configuration and a cylindrical anode. The results have identified three different modes of the arc instabilities: steady, takeover and restrike mode, presented in Figure 1.29. The numerical simulations, given by [27, 28, 56–58], have showed that the plasma instabilities have been mainly related to the elongation of electrical current paths due to the plasma flow and Lorentz forces. Duan and Heberlein have determined the mixed modes related to the combinations of the restrike and takeover modes or the takeover and steady modes [27]. The steady mode has been achieved with a high level of the arc current, 900 A, and a pure argon flow [27]. This mode corresponds to very small arc voltage fluctuations: $\Delta U_{arc} = \pm 0.5V$ due to the balance between the drag force of the plasma gas and the electromagnetic forces. The steady mode is characterized by a nearly fixed position of the anode attachment, what causes the rapid erosion of the anode.
The takeover mode appears mostly by using the monatomic plasma gases [25, 59]. It has been called takeover because a new attachment gradually "takes over" the role of the old attachment, instead of being created by the breakdown mechanism. The takeover mode is characterized by a periodic or quasi-periodic voltage fluctuations, shown in Figure 1.29.

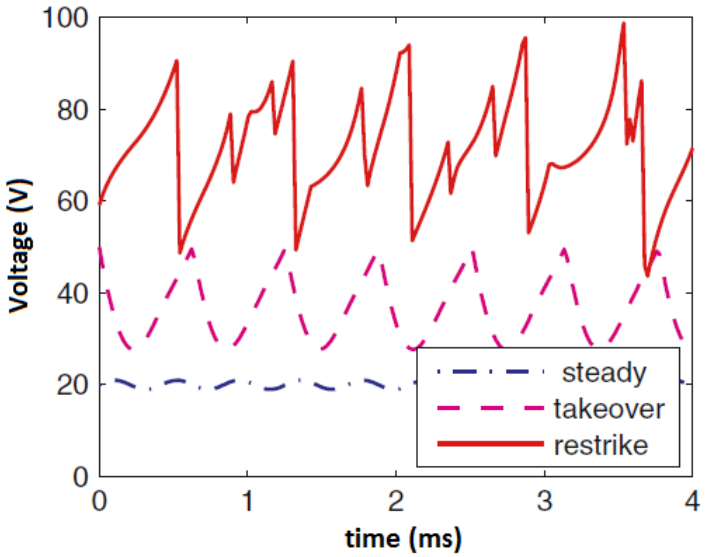


**Figure 1.29:** Arc voltage traces corresponding to different anode attachment modes in a dc torch [57].

The restrike mode is characterized by the highest voltage fluctuations and a sawtooth shape profile of the voltage trace. An arc operating in this mode is very unstable. It results in the increase of the arc voltage and sudden drop when a new current path is created by an electric breakdown (re-strike). This mode will be described in details in the following section.

Duan and Heberlein have determined the method to characterize the arc instabilities modes presented above [27]. It is based on the analysis of the voltage waveform, shown in Figure 1.30.

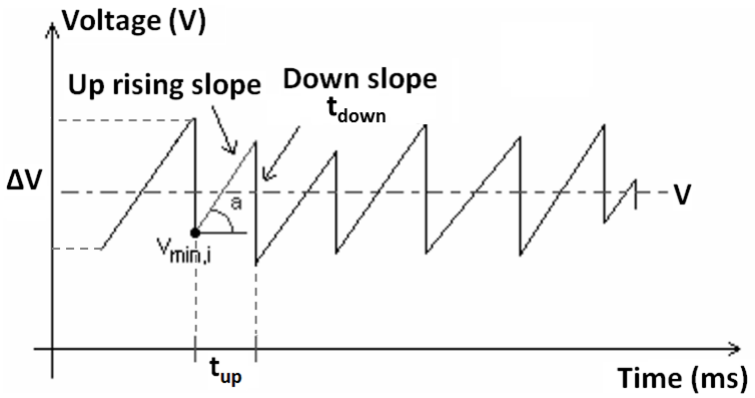


**Figure 1.30:** Arc voltage waveform used to distinguish the torch operation modes.

To separate the restrike mode from takeover mode, the shape of the voltage waveform,

characterized by a shape factor S, is determined by the following equation:

$$S = \frac{t_{up}}{t_{down}} \tag{1.48}$$

where:

$t_{up}$ is the duration time of the waveform up-rising slope,
$t_{down}$ the duration time of the down slope, highlighted in Figure 1.30.

The fluctuation amplitude is used to distinguish the takeover mode from the steady mode. The amplitude factor, A, is calculated as follows:

$$A = \frac{\Delta V}{V} \times 100\% \tag{1.49}$$

where:

$\Delta V$ is the amplitude of the arc voltage fluctuation,
$V$ the mean arc voltage.

The arc mode is defined as running in restrike mode when A $\geq$ 10% and S $\geq$ 5. If A $\geq$ 10% and S $<$ 1.1, the arc is determined as running in takeover mode and for A $<$ 2% the arc is in a steady mode [27].
The origins of the arc instabilities should be divided into two sections according to the time scale. The presented modes of the fluctuations are associated with the short time scale evolution of the voltage.
Moreover, the drifting of the arc voltage can be explained by the erosion and wear of electrodes, what is shown in Figure 1.31 and belongs to the group of the long time evolution of voltage. Figure 1.31 presents the time dependence and corresponding power spectra of voltage fluctuations. The use of worn electrodes results in the increase of arc fluctuations.

The cathode erosion is due to the diffusion and evaporation of thoria. It results in a lower flow velocity of the plasma by the decrease of the current density of arc attachment at the cathode. The erosion of the anode is caused by the strong heat fluxes of arc attachment between the arc column and the anode surface. It is observed as a voltage drop which increases drastically after a few tens of hours working time and results in the ejection of tungsten or copper particles to the plasma jet, what is damaging the coating.

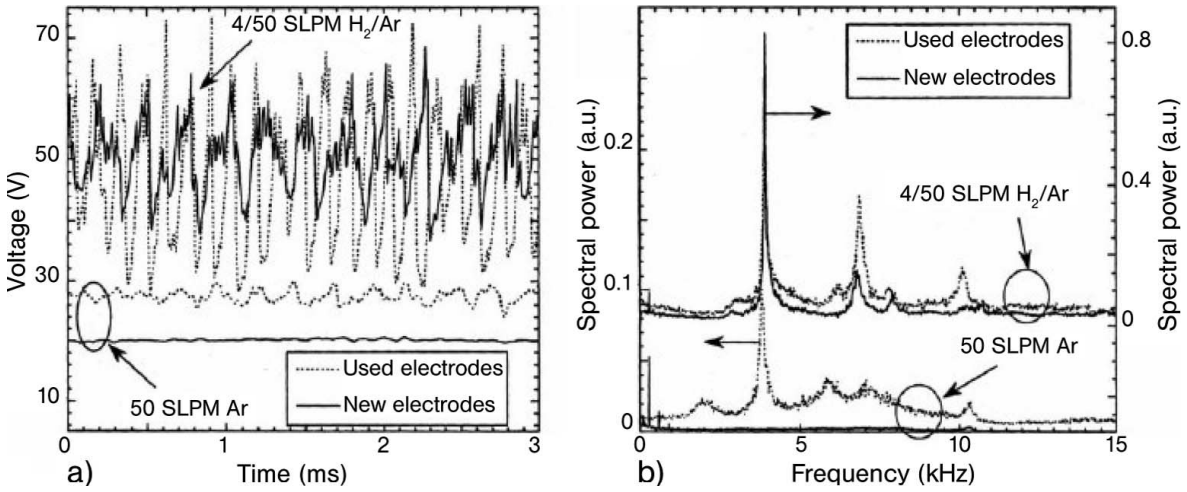


**Figure 1.31:** Time dependence (a) and corresponding power spectra (b) of the voltage fluctuations for new and used electrodes. Plasma parameters: 50 slpm Ar and 4/50 slpm $H_2$/Ar, 500A [60].

### 1.3.2.1 Restrike mode

As has been mentioned above, the arc column expands itself from the cathode tip and is surrounded by a cold gas boundary layer. Through this layer the electrical connection with the anode wall is carried out by an arc loop which is exposed to the drag and electromagnetic forces. The imbalance between these forces causes that the drag force, which is the result of the interaction of the incoming gas flow over the arc, induces the stretching and lengthening of the arc column, presented in Figure 1.32 a).

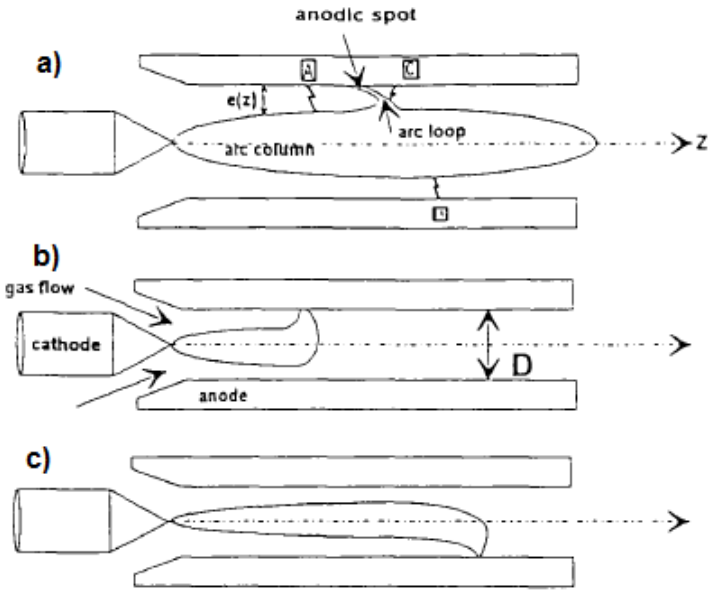


**Figure 1.32:** Schematic view of Restrike model: a) the arc column at the end of a lengthening process, b) after an upstream restrike, c) after a downstream restrike [61].

This process is accompanied by the rise of the arc voltage which corresponds to an increase of the electrical current path in the direction of the superimposed flow during $\tau_i = t_{i+1} - t_i$ in Figure 1.33.

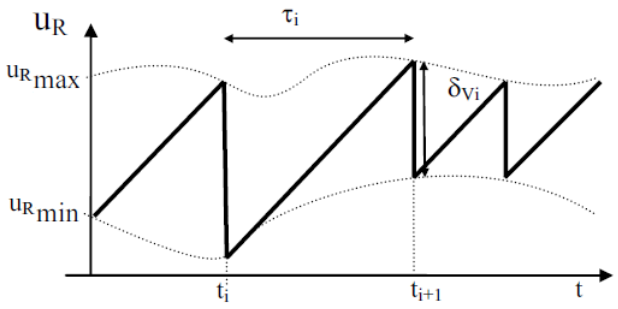


**Figure 1.33:** Temporal evolution of the arc voltage corresponding to restrike mode.

The lengthening process is followed by an electrical breakdown at $t_{i+1}$ in Figure 1.33. It leads to the creation of new arc root, what corresponds to a minimum arc voltage $U_{Rmin}$ and is identified with a voltage jump $\delta_{Vi}$. Coudert *et al.* have highlighted that the voltage breakdown, defined as $V_b(Z)$, is related to the thickness of the cold gas boundary layer, $e(Z)$, as follows: $V_b(Z) = e(Z).E_b$, where $E_b$ is the breakdown field [61], which has been determined up to now by Paschen's law. However, the results presented in Chapter 2 have highlighted that due to the magnitude of this field, it can not be attributed to Paschen's law but is divergently referred to the thermal instabilities [V. Nemchinsky private communication]. The restrike arc voltage is depicted as: $V_r(t) = U_a + U_c + V_c(Z_{i-1}) + V_l(t)$, for $t_{i-1} < t < t_i$, where $U_a$ and $U_c$ are respectively the anode and cathode falls, presented in Figure 1.34, $V_c(Z_{i-1})$ is the voltage drop along the arc column which depends on the arc root location, $Z_{i-1}$, $V_l(t)$ the voltage drop along the arc loop connecting the column to the anode wall. Assuming that just after the spot creation, at time $t_{i-1} + \varepsilon$, the arc voltage is defined by:

$$V(t_{i-1} + \varepsilon) = V_m(t_{i-1}) = V_c + V_a + V_c(Z_{i-1}) \tag{1.50}$$

and the voltage just before the further breakdown giving rise to a new arc root location, $Z_i$, at time $t_i - \varepsilon$, is determined by the equation:

$$V(t_i - \varepsilon) = V_c + V_a + V_c(Z_{i-1}) + V_l(t_i - \varepsilon) \tag{1.51}$$

the voltage jump, $\delta_{Vi}$, occurring at $t_i$, is given by:

$$\delta_{Vi} = V(t_i - \varepsilon) - V(t_i + \varepsilon) = V_l(t_i - \varepsilon) + V_c(Z_{i-1}) - V_c(Z_i) \tag{1.52}$$

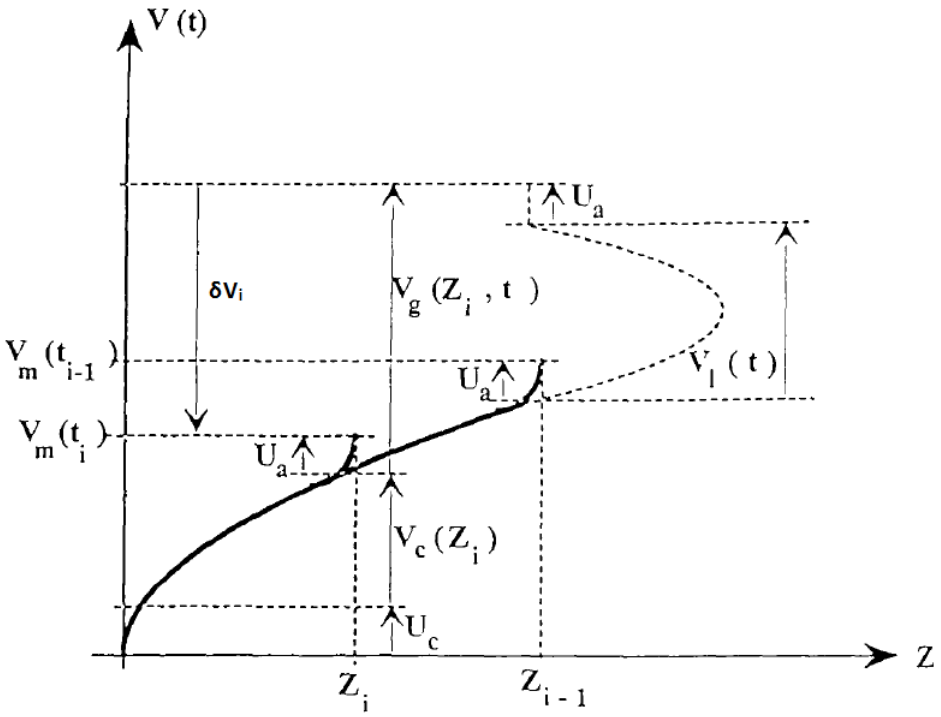


**Figure 1.34:** The arc voltage evolution [61].

### 1.3.2.2 Improvement of plasma spray process

For many years, the special efforts have been made to understand and improve the control of suspension plasma spray processes. In particular, the plasma unsteady characteristics which result in a poor reproducibility and reliability of the method. The following section focuses on the improvement methods of the plasma spray process concerning the plasma instabilities.

#### 1.3.2.2.1 New designs of dc plasma torch

Development of new plasma torches is driven by the need to improve stability and to increase the range of powders to be used. A large number of the thermal plasma torches have been designed [19,62]. The following section describes the recently developed torches: Triplex and Axial III.

- **Triplex (Sulzer Metco, Switzerland)**
  In the mid-1990s Sulzer Metco developed a new plasma gun concept in the co-operation with the Universitat der Bundeswehr, Munich (University of the Federal Armed Forces). The result is the Triplex gun, a three-cathode plasma spray torch with cascading nozzle and anode end ring, presenting in Figure 1.35 [63, 64].

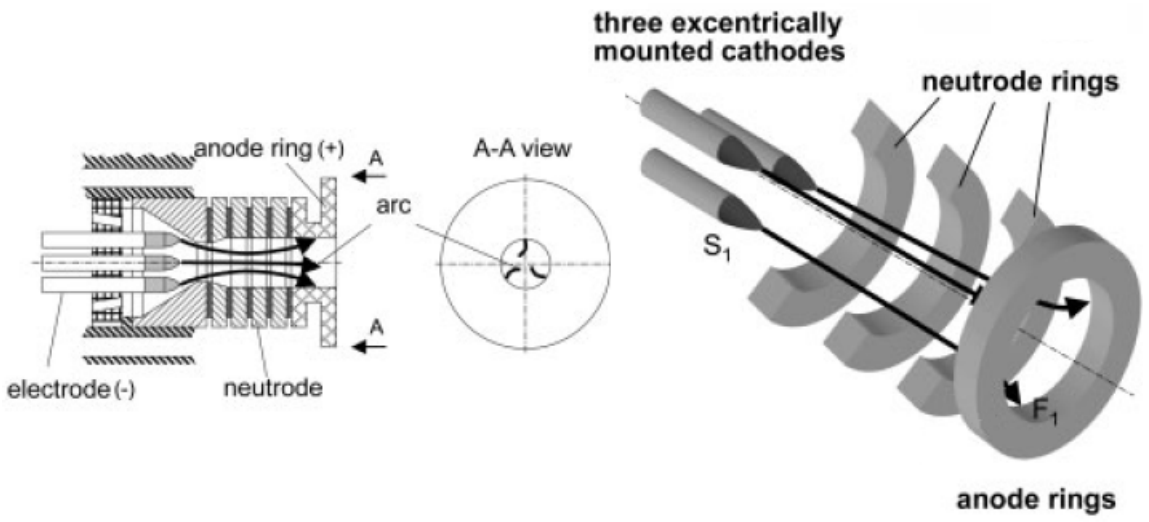


**Figure 1.35:** The schematic view of the Triplex torch [64].

It consists of three water cooled parallel cathodes insulated against each other and supplied by independent power sources. The electrical energy is distributed through three parallel arcs striking at a single anode with three separate anode attachments, what has solved the problem of increased anode erosion (the voltage loss equals to 1-5% over 90h working time). To prevent the instability of the anode attachments the nozzle is consisted of several rings electrically insulated, except of the last one which operates as an anode. Schein *et al.* have shown that the conventional dc torch, F4, produces a very unstable plasma jet with large variations in the jet length, presented in Figure 1.36 a). This characteristic Triplex construction results in the elongation of the arcs and a much more stable plasma jet, what is shown in Figure 1.36 b).

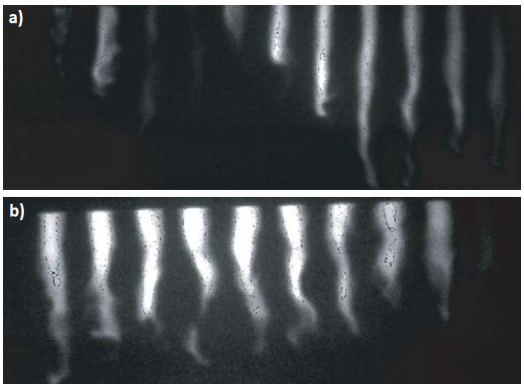


**Figure 1.36:** Pictures of the plasma jets obtained by: a) F4 (exposure time 5 ns, 6 mm nozzle, current: 540 A, plasma gas: 45 slpm Ar and 12 slpm $N_2$), b) Triplex (exposure time 3 ns, 9 mm nozzle, current: 350 A, plasma gas: 45 slpm Ar) [63].

Triplex torch allows obtaining higher arc voltage and enthalpy of the plasma jet. It is able to achieve the voltages of 80-120 V (with arc currents limited to 300 A and Ar-He plasma forming gases) compared to 40 V obtained by the conventional dc torch.

Another advantage of Triplex torch is the temperature distribution produced at the nozzle exit. As it can be observed in Figure 1.37 the plasma jets are constituted of three lobes, the zones with higher and lower gas viscosity.

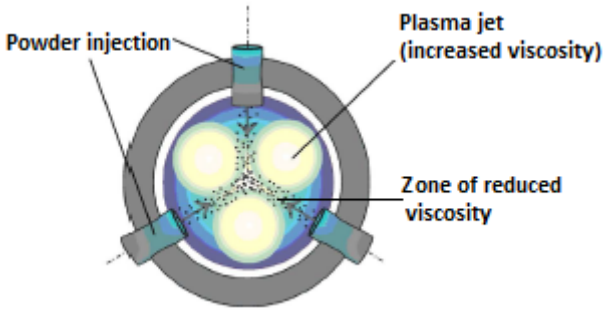


**Figure 1.37:** Schematic view of the powder injection into Triplex torch [51].

Thus the powder injection into the central region of the plasma jet (the zone with high viscosity) is more easily achieved along one of the canals where the gas viscosity is reduced (Figure 1.37). It allows obtaining a better interaction of the particles with the plasma flow what leads to improved coatings.

- **Axial III (Northwest Mettech Corp., Canada)**

  Axial III consists of three cathodes and three anodes, arranged such that their axes are parallel, presented in Figure 1.38. They are operated by three power supplies (total power ranging from 50 to 150 kW) and generally they work with Ar-$N_2$-$H_2$ or Ar-$N_2$-He gas mixtures.

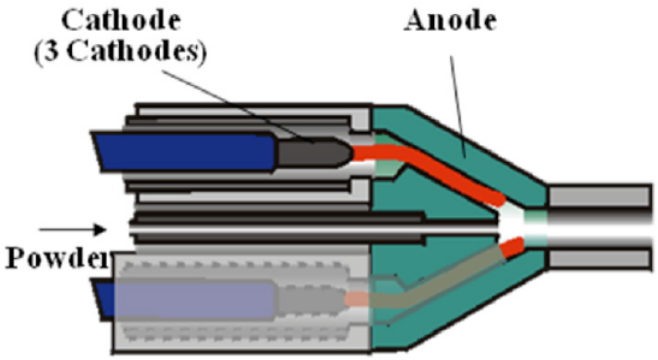


**Figure 1.38:** Schematic view of Axial III [65].

The AxialIII configuration allows producing three plasma jets which converge together in a common nozzle. The feedstock material is injected axially between these three plasma jets, what permits to obtain the particle trajectories more homogeneous and a longer residence time of the feedstock material in the plasma zone. Moreover, as these three plasma jets fluctuate independently, voltage fluctuations have lower effects on the axially injected feedstock material.

#### 1.3.2.2.2 Reduction of plasma instabilities

The studies of the instabilities of the plasma jet have resulted in the methods to reduce these fluctuations.

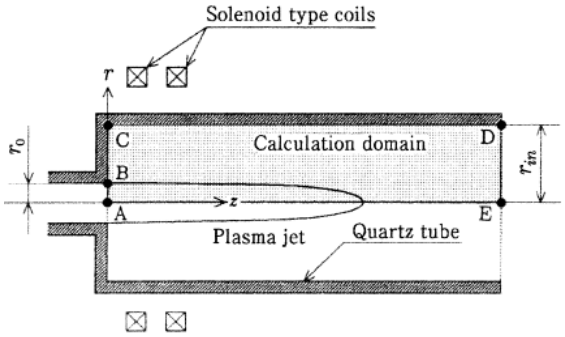


**Figure 1.39:** Schematic view of the plasma jet stabilized by magnetic field [66].

Nishiyama *et al.* have highlighted the possibility of the stabilization of unstable plasma jet behaviour by applying magnetic field [66, 67]. Figure 1.39 shows the schematic model of this method. The plasma jet has been issued into a quartz tube. Two solenoidal coils have been placed at the nozzle exit to produce a mirror type magnetic field. The maximum magnetic flux density, $B_{z_{max}}$, was equal to 0.44 T. The pure argon (20 slpm) plasma was tested supplied by the power of 8 kW. The temperature and velocity for each plasma species with and without magnetic field were measured, what is presented in Figure 1.40. By applying the magnetic field it is possible to increase the temperatures of all plasma

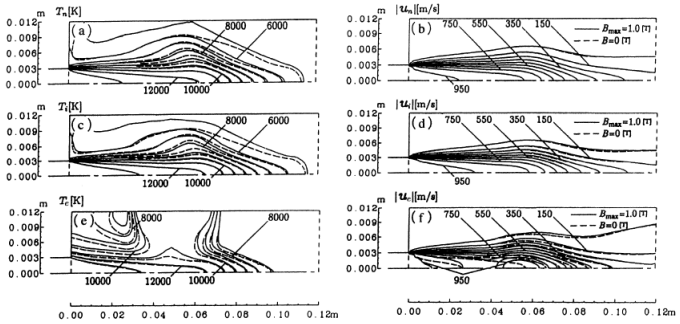

**Figure 1.40:** Isocontours of temperature and velocity of the heavy species ($T_n, T_i$ and $U_n, U_i$) and of the electrons ($T_e$ and $U_e$) with and without applied magnetic field [66].

species outer from the jet fringe. In addition the electron velocity is changed considerably in the central region by Lorentz force in the magnetic field. The results have shown that the application of magnetic field can control the electron velocity and the temperature in the plasma jet.

## 1.4 Conclusions

The relatively new method, suspension plasma spraying, allows producing finely structured nano-sized coatings, what expands its application area to e.g. thermal barrier coatings (TBCs), solid oxide fuel cell (SOFC), photo-catalytic coatings. However, the results of the examination of coatings microstructures by SEM or the studies of the suspension fragmentation according to the arc voltage fluctuations have highlighted the difficulties encountered in this method. The large discrepancies in the particles trajectories and the heat transfers, the plasma instabilities result in the insufficient reproducibility and reliability of the SPS method. Therefore, for many years the special efforts have been made to improve this process. One of the solutions is to develop new non-conventional plasma torch. However, as the coating microstructure has highlighted, the plasma produced by these torches still remain non-uniform resulting in non-homogeneous microstructure of the coatings. Consequently, the following dissertation will present a new approach to arc fluctuations by the increase of the instabilities in a controlled way to obtain a pulsed arc plasma jet with a synchronous injection of materials. This process requires an understanding of the origin of arc instabilities. Therefore, the next chapter will present the studies of the plasma fluctuations in the conventional dc torch.

# Part I

# Résumé du chapitre 1

Cette thèse présente le procédé de projection par plasma d'arc produit par une torche plasma à courant continu (dc en anglais) à la pression atmosphérique. Selon la matière injectée dans le jet de plasma, la technique de projection par plasma peut être classée dans plusieurs catégories: la projection dans l'air à pression atmosphérique (APS, Atmospheric Plasma Spraying en anglais) en utilisant la poudre comme la matière injectée, la projection de solution (SPPS) et de suspension (SPS). Dans le procédé APS, les particules de poudresont injectées dans le jet de plasma. L'épaisseur minimale des revêtements est limitée à environ 10 $\mu$m [7]. Ils sont principalement utilisés pour fournir une protection contre les températures élevées, la corrosion, l'érosion et l'usure. Le procédé SPPS, décrit par Karthikeyan *et al.* [8], est la méthode de projection de solution, dans lequel au lieu d'utiliser une poudre, un précurseur en solution aqueuse est injecté dans le jet de plasma. Ce procédé permet d'obtenir une microstructure des revêtements nano et micrométrique. Une méthode relativement nouvelle est la projection par plasma de suspension, qui a été inventée par l'Université de Sherbrooke au milieu des années 1990 [9]. La suspension est composée de particules de poudre micro- et nano-métriques dispersées dans un liquide. Le procédé SPS permet produire les revêtements finement structurées, voire de taille nanométrique, ce qui donne la possibilité d'étendre le domaine d'application des couches. Ils peuvent être utilisés en tant que:

- Pile à combustible à oxyde solide (SOFC en anglais)
- Barrières thermiques
- Dépôts catalytiques

Le plasma, appelé aussi le quatrième état de la matière, est un gaz électriquement conducteur en raison de la présence de particules chargées: les ions et les électrons. La thèse suivante décrit le plasma thermique produit par une décharge électrique à fort courant continu. Une torche à plasma transforme l'énergie électrique fournie par un générateur de courant en énergie thermique par effet Joule au sein d'un gaz plasmagène en contact avec un arc électrique. Cet arc électrique est créé entre une cathode, pôle négatif, et une anode, pôle positif, et soufflé par les gaz plasmagènes qui sont injectés en amont de la torche entre les deux électrodes.
La torche à plasma d'arc à courant continu comporte trois éléments essentiels: la cathode, l'anode et l'injecteur de gaz.

- **Cathode**
  Elle permet de fournir les électrons à l'arc électrique. Les paramètres de la cathode sont différents en fonction des mécanismes d'émission d'électrons. Dans le cas de la cathode chaude, les électrons sont fournis par l'émission thermoionique, suivant la loi de Richardson-Dushman, Equation 1.1. $1-2$ % en masse de $ThO_2$; 2 % en masse de

$La_2O_3$, $Y_2O_3$, $CeO_2$. Le rôle de dopant est d'abaisser la fonction de travail thermoionique de tungstène. Deux types de cathodes chaudes sont généralement utilisés: les électrodes tiges et les électrodes boutons.

- **Anode**
  L'anode a un rôle passif qui consiste à collecter les électrons. Elle est soumise à des flux thermiques très élevés (jusqu'à 160 $W.mm^{-2}$) au point d'accrochage de l'arc électrique. Par conséquent, elle doit être refroidi à l'eau et fabriquée en cuivre ultra-pur (OFHP Oxygen Free High Purity), caractérisé par une forte conductivité thermique: 358 $W.m^{-1}.K^{-1}$ et la diffusivité thermique: 1114 $10^{-6}$ $m^2.s^{-1}$ à 25°C, avec parfois un gainage en tungstène.

- **Injecteur de gaz**
  Il existe trois méthodes principales d'injection: l'injection swirl, l'injection radiale et l'injection axiale. Dans l'injection axiale le gaz est injecté parallèlement à l'axe de l'anode et possède une composante de vitesse longitudinale. Dans le cas de l'injection radiale la bague d'injection est percée de trous perpendiculaires à l'axe de la torche. La vitesse des gaz présente donc une forte composante radiale qui diminue ensuite. Dans le cas de l'injection swirl, le gaz possède une composante de vitesse initiale axiale et radiale.. Les tourbillons formés créent des forces centrifuges, ce qui pousse le gaz froid vers les parois de la torche.

Le jet de plasma est produit par une torche dans laquelle l'arc électrique est établi entre une cathode et une anode. La colonne d'arc est développée à partir de la tête de cathode est caractérisée par un écoulement laminaire qui est délimité par une enveloppe isotherme ($T_c > 7500K$) à l'intérieur de laquelle la conductivité électrique des gaz est suffisamment élevée pour permettre le passage du courant. En dehors de cette zone, la conduction électrique est négligeable, ce qui apparaît comme la couche limite froide. L'épaisseur de cette couche dépend fortement des paramètres du procédé: le courant d'arc, le diamètre interne de la tuyère, l'injection de gaz formant le plasma. L'accrochage de l'arc à la paroi de la tuyère est perpendiculaire à la surface de l'anode et il est sous la forme d'une colonne de gaz à haute température et à basse densité traversant la couche limite de gaz froid. Les études sur le pied d'arc ont montré que ce point d'accrochage se déplace continuellement. Ceci est dû à des mouvements axiaux et de rotation induits par les forces dynamiques (force de traînée) liées à l'écoulement du gaz, les forces électromagnétiques de Lorentz dues à l'interaction entre le courant d'arc et le champ magnétique induit par ce courant, et les effets thermiques. Quand le jet de plasma, caractérisé par une faible densité et une vitesse élevée (entre 600 et 2200 m/s), sort de la tuyère de la torche, il se mélange avec l'atmosphère environnante. Cela entraîne donc des forces de cisaillement qui vont se traduire par la création d'anneaux tourbillonnaires.

Le plasma produit par la torche à courant continu est supposé à équilibre thermodynamique local (Local Thermal Equilibrium LTE en anglais). Le plasma thermique est considéré comme optiquement mince et donc le rayonnement ne correspond pas au rayonnement du corps noir. Cela signifie que la loi de Planck n'est pas valable dans LTE. Les processus de collision doivent être localement en équilibre. Par conséquent, les populations de toutes les espèces et leurs niveaux excités sont décrits par les équations de Maxwell, Boltzmann, Saha et Guldberg-Waage, présentés dans le chapitre 1, mais avec la température qui peut varier dans le temps et l'espace.
Les principaux gaz rencontrés en projection thermique sont l'argon (Ar), l'hydrogène ($H_2$), l'hélium (He) et l'azote ($N_2$). Le choix du gaz injecté joue un rôle important dans la technique, il définit les propriétés thermodynamiques et de transport importantes des plasmas: l'enthalpie, la conductivité électrique, la viscosité et la conductivité thermique.
Dans le procédé de projection conventionnelle (APS) les poudres avec des diamètres généralement entre 10 $\mu$m et 110 $\mu$m sont injectées au jet de plasma. L'injection de la matière est effectuée principalement par un tube de diamètre interne de 1.5 - 2 mm. Les particules de poudre sont transportées par le gaz, par exemple l'argon, à la vitesse d'écoulement entre 3 et 10 slm. Dans le cas des torches à plasma à courant continu classiques, le matériau est introduit dans le jet de plasma radialement. L'injection axiale est réalisée dans les nouvelles conceptions de la torche, par exemple Axial III. La thèse suivante se concentre sur les études de la torche plasma en courant continu associés à l'injection de suspension.
La suspension appropriée pour le procédé SPS se compose généralement: de poudres submicronique ou nanométriques, de solvant et d'additifs chimiques. Les poudres sont principalement produites par les procédés de précipitation chimique, de broyage mécanique, des traitements thermiques. Le choix du solvant est très important pour les propriétés de la suspension, par exemple pour avoir unefaible viscosité et une bonne stabilité. Les principaux solvants utilisés dans la production de la suspension sont l'eau et l'éthanol. En comparant les propriétés de ces deux liquides, on peut dire que l'eau nécessite plus d'énergie que l'éthanol pour vaporiser. En plus, l'éthanol est caractérisé par une tension de surface inférieure. Néanmoins, il contient du carbone qui peut polluer les revêtements. Par conséquent, le mélange de l'éthanol avec de l'eau sont couramment utilisés. Pour obtenir une bonne homogénéisation et désagglomération de la suspension une agent dispersant est généralement ajouté pour stabiliser la poudre dans le solvant, par exemple un ester de phosphate. En ajoutant par exemple de l'ammonium d'acide polyacrylique (PAA) ou de l'alcool polyvinylique (PVA), il est aussi possible de modifier la tension de surface ou la viscosité de la suspension.
Il existe deux grandes familles d'injection de suspensions: l'atomisation et l'injection mécanique.

Le principe de fonctionnement de l'atomiseur est basé sur l'application de pulse de gaz sous pression, contrôlée par l'action d'une électrovanne, sur le liquide contenu dans un réservoir. Le liquide est éjecté par la buse et forme un spray de gouttelettes. Il est à noter qu'un gaz d'atomisation peut être utilisé pour atomiser un jet de liquide en gouttelettes. Il a été montré que les liquides caractérisés par la viscosité comprise entre 0.1 et 50 à 60 mPa.s se fragmentent en gouttelettes en fonction du nombre de Weber, $We$, qui est le rapport entre la force exercée par l'écoulement du liquide à la force de tension de surface, définie par l'équation 1.12. Pour les liquides à viscosité élevée le nombre Ohnesorge, $Oh$, doit aussi être considéré. Il concerne les forces visqueuses et les forces de tension de surface et d'inertie, selon l'équation 1.13. Les dimensions typiques des gouttelettes atomisées de la matière sont comprises entre 2 et 100 $\mu$m, les vitesses correspondantes variant de 5 à 60 m/s.

Dans le cas de l'injection mécanique, la suspension est stockée dans un réservoir sous pression et injectée à travers une buse de diamètre interne spécifiée, $d_n$. Fazilleau *et al.* ont utilisé un diaphragme de buse calibrée au diamètre de 150 $\mu$m fabriqué par l'électro-érosion et Etchart-Salas *et al.* ont présenté des résultats obtenus par la buse d'un diamètre variant de 300 $\mu$m, usiné par laser. Les études ont montré que le carré de la vitesse du liquide varie de façon linéaire avec la pression du réservoir. Par exemple, les vitesses d'injection entre 25 et 35 m/s ont été obtenues avec une pression d'air comprise entre 0,2 et 0,6 MPa.

Lorsque le jet de la suspension ou les gouttes sont injectées dans le jet de plasma, ils sont progressivement ou rapidement fragmentés en gouttelettes. Ce processus de fragmentation conduit à la diminution de leur volume, ce qui entraîne que la diminution de leur quantité de mouvement. Fazilleau a présenté les conditions favorables pour une bonne pénétration de la suspension dans le jet de plasma définie par l'équation 1.17. Quand les gouttelettes de la suspension sont entraînées en jet de plasma, elles sont soumises à la fragmentation en raison d'une forte contrainte de cisaillement (générée par l'écoulement du plasma) et la vaporisation du liquide due à haut flux thermique du plasma. Il a été démontré que la fragmentation de la suspension dépend du nombre de Weber, We. Le nombre de Weber d'environ 14 est la valeur critique pour laquelle la goutte est fragmentée

Une goutte dans un écoulement de plasma est soumise à deux forces principales, la force aérodynamique et la force de tension de surface. La force aérodynamique du jet de plasma permet la désintégration de la goutte, et la tension de surface du liquide s'y oppose. En égalant ces deux forces, le diamètre minimum, $d_f$, de ces micro-gouttes, lorsque la fragmentation est terminée, peut être déterminé par la formule 1.20. Le paramètre important de la fragmentation est la durée de ce processus. Fazilleau *et al.* ont montré que le temps de fragmentation, $t_f$, est donnée par l'équation 1.21.

Le flux de chaleur du plasma transmis par convection à la goutte, permet l'évaporation

complète de celle-ci après un temps, $t_v$, défini par l'équation 1.23. Il est intéressant de comparer ce temps avec le temps de fragmentation de la goutte. Les résultats présentés sur la figure 1.19 montrent que le temps de vaporisation est deux ordres de grandeur plus élevé que celui de la fragmentation. Le phénomène de fragmentation se produit donc toujours avant la vaporisation complète du solvant.

L'équilibre entre la conduction et la convection thermique ($Q_{CV}$) du gaz chaud vers la particule et son refroidissement en raison des pertes de chaleur rayonnante de la surface ($Q_R$) et les pertes de rayonnement vapeur ($Q_V$) détermine le transfert de chaleur net à une particule ($Q_{net}$). Les mécanismes de conduction et de convection sont généralement décrits par le nombre de Nusselt, Nu, défini par 1.255. Dans le cas des particules de la suspension de dimensions nanométriques ou sub-micrométriques l'effet de Knudsen, qui réduit les transferts de chaleur, devrait être également pris en considération. Il dépend du nombre de Knudsen, Kn, déterminée par l'équation 1.28. Dans le cas des particules de moins de 0.1 $\mu$m, la force de thermophorèse doit être prise en compte dans les zones caractérisées par des gradients de température. Les petites particules changent leurs trajectoires du coeur du plasma à la périphérie du jet, caractérisée par des températures et des vitesses de gaz inférieures. En outre, en raison de leur faible inertie, les particules peuvent suivre la trajectoire de gaz chaud qui s'écoule parallèlement à la surface du substrat et ne jamais avoir un impact sur cette surface, ce qui se produit lorsque le nombre de Stokes St est inférieur à 1. Le nombre de Stokes caractérise le comportement des particules en suspension dans un écoulement de fluide et il est déterminé par l'équation 1.311.

Lorsque les particules sont caractérisées par St$>$ 1, elles peuvent traverser la couche limite qui se développe à la surface du substrat. Ces particules frappent et s'aplatissent sur le substrat, ou sur un matériau précédemment déposé, en formant des lamelles (splat). La structure de la lamelle résulte de l'étalement et de la solidification des particules sur le substrat, ce qui dépend des paramètres suivants: la vitesse et la taille de particule, les propriétés du matériau de la particule à l'état liquide, par exemple, la viscosité, la tension superficielle, la mouillabilité du substrat par des particules liquides, l'angle de l'incidence par rapport au substrat, la rugosité de surface du substrat.

Le temps d'étalement d'une lamelle est de l'ordre de quelques $\mu$m. Le procédé de solidification est plus longue et commence avant l'étalement est terminé. Le temps entre deux lamelles successives est de l'ordre de dix à quelques dizaines de $\mu$s. Par conséquent, la prochaine particule frappe sur une lamelle déjà solidifiée.

Comme mentionné ci-dessus, dans le procédé de projection par plasma la plupart des torches sont alimentées par une source d'alimentation en courant continu. Toutefois, le jet de plasma produit par une torche présente des caractéristiques instationnaires. Les études ont permis de vérifier que ces fluctuations du plasma ont une forte influence

sur les processus de la fragmentation et la vaporisation des gouttelettes, en particulier dans la technique récemment développée, la projection par plasma d'arc de suspension. Il en résulte une mauvaise reproductibilité et la fiabilité du procédé, ce qui cause des applications limitées de la projection par plasma. En analysant les variations de la tension d'arc modes suivants ont été identifiés:

- **Le mode stable ("steady mode")**
  Ce mode de fonctionnement est observé avec un haut niveau de courant d'arc, 900 A, et un argon pur (par exemple débit d'argon de 60 L/min). Le mode stable correspond à de très faibles variations de tension de l'arc: $\Delta U_{arc} = \pm 0.5V$ en raison de l'équilibre entre la force de traînée du gaz de plasma et les forces de Lorent. Le mode stable est caractérisé par une position fixe du pied d'arc, ce qui provoque l'érosion rapide de l'anode.

- **Le mode oscillant ("takeover mode")**
  Ce mode apparaît surtout en utilisant les gaz de plasma monoatomiques. Le mode "takeover" est caractérisé par les fluctuations périodiques ou quasi-périodiques de la tension. Ce mode a été appelé "takeover", car le nouveau pied d'arc naît pendant que l'ancien s'éteint progressivement.

- **Le mode claquage-réamorçage ("restrike mode")**
  Le mode claquage-réamorçage correspond aux fluctuations de tension plus élevées. Le signal de tension présente une forme caractéristique en dents de scie avec de fortes fluctuations de tension. Le déséquilibre entre la force de traînée et de force électromagnétique induit l'étirement et l'allongement de la colonne d'arc qui est accompagnée par l'augmentation de la tension d'arc. Le processus d'allongement est suivi par un claquage électrique au travers de la couche limite entre la colonne d'arc et la paroi anodique. Un nouveau point d'accrochage est créé en amont dans la tuyère, ce qui correspond à une tension d'arc minimale et est identifiée par un saut de tension.